FFI-rapport 2011/00007

Channel sounding for acoustic communications: techniques and shallow-water examples

Paul van Walree

Norwegian Defence Research Establishment (FFI)

11 April, 2011

FFI-rapport 2011/00007

1146

P: ISBN 978-82-464-1901-5
E: ISBN 978-82-464-11902-2

Keywords

Kanalmålinger

Kanalsimulering

Akustisk kommunikasjon

Approved by

Connie Elise Solberg	Project Manager
Elling Tveit	Director of Research
Jan Erik Torp	Director

English summary

This report deals with channel soundings, which are measurements of the time-varying impulse response of a propagation medium. The treatment focuses on underwater acoustic channels, the characterization of which is becoming increasingly important to support developments in the fast growing field of underwater communications and networking. The benefits of channel sounding include increased understanding of channel physics and modem performance, validation of channel models, and support for the establishment of standard test channels. Channel models are of crucial importance in communication transceivers and channel simulators.

The report creates awareness of the risk of measurement errors related to properties of the probe signal, such as aliasing and delay-Doppler coupling. Channel parameters are defined and numerous shallow-water example soundings are reviewed. There are many conclusions, the most important one perhaps being that there is no typical or average acoustic channel. The variation in statistical properties, delay spread, and Doppler spread is immense. This variation is not only found between geographical areas and seasons, but also on smaller scales. For instance, the examples show that a wind burst or a passing ship can completely alter the scattering properties of a channel.

Doppler spectra are examined for wideband and narrowband waveforms. In agreement with our previous work, the basic shape of measured spectra appears to be well characterized by stretched and compressed exponentials. The spectral width increases with the frequency, something that should be kept in mind upon applying narrowband tools and models to broadband waveforms. An empirical relationship is established that reduces the stretched-exponential spectrum to a single parameter.

The present report is useful in several ways. It can be used as a guide for channel soundings at sea, including straightforward signal processing and computation of channel parameters. It also helps to recognize measurement errors and other pitfalls. Parameterization of Doppler spectra is useful for stochastic channel modeling. Most importantly, however, the collection of example soundings emphasizes the wide variety of acoustic propagation channels. It illustrates the challenge to devise communication systems that are efficient and robust to the environment, as well as channel simulators that faithfully mimic these environments. On the other hand, the set of channels in this report is selected so as to demonstrate the diversity as a function of area, season, weather, and local disturbances. One is unlikely to encounter all these channels for a given application or mission.

Sammendrag

Denne rapporten omhandler kanalmålinger, det vil si målinger av den tidsvarierende impulsresponsen til et propagasjonsmedium. Fokuset er på den undervannsakustiske kanalen. Karakterisering av slike kanaler er blitt stadig viktigere for å støtte utviklingen i det hurtig voksende feltet undervannskommunikasjon og nettverk. Kanalmålinger muliggjør øket forståelse av kanalfysikk og modemytelse, validering av kanalmodeller, og understøttelse for iverksetting av standard testkanaler. Kanalmodeller er av stor betydning i kommunikasjonssendere, -mottakere og kanalsimulatorer.

Rapporten belyser risikoen for målefeil, som folding og forvrengning på grunn av kopling mellom tidsforsinkelse og Doppler, og relaterer disse til probesignalets egenskaper. Videre defineres kanalparametre, og en rekke eksempler på gruntvanns-kanaler gjennomgås. Det er mange konklusjoner, den viktigste er muligens at det ikke eksisterer noen typisk eller gjennomsnitts akustisk kanal. Variasjonen i statistiske egenskaper, tidsspredning og Dopplerspredning, er enorm. Disse variasjonene finnes ikke bare mellom ulike geografiske områder og årstider, men også på mindre skalaer. For eksempel kan et vindkast eller et passerende skip fullstendig forandre spredeegenskapene til en kanal.

Dopplerspektra er studert for både bredbånds- og smalbåndsbølgeformer. Formen på målte spektra viser seg å kunne beskrives godt ved en strukket/komprimert eksponentiell funksjon. Dette er i samsvar med de tidligere resultatene våre. Den spektrale bredden øker med frekvens, noe en bør være oppmerksom på ved anvendelse av smalbåndsmetoder og modeller på bredbåndssignaler. En empirisk sammenheng er etablert, som reduserer antall parametre i det eksponentielle spektret til en enkelt parameter.

Rapporten kan benyttes på flere måter: Den kan brukes som en guide for å gjøre kanalmålinger i sjøen, inkludert basis signalbehandling og beregning av kanalparametre. Den kan også være til hjelp for å gjenkjenne målefeil og andre feller. Parametrisering av Doppler spektra er nyttig for stokastisk kanalmodellering. Men viktigst er det at samplingen av eksempler viser den store variasjonen som finnes i akustiske propagasjonskanaler. Eksemplene illustrerer utfordringen ved å konstruere kommunikasjonssystemer som er robuste og effektive med hensyn på det akustiske miljø, og kanalsimulatorer som troverdig reproduserer disse miljøene. På den annen side er eksemplene i denne rapporten valgt for å vise variasjonsbredden i akustiske kanaler som funksjon av område, årstid, værforhold, og lokale forstyrrelser: det er lite sannsynlig at en møter alle disse kanalene i en gitt anvendelse eller misjon.

Contents

1 Introduction

There is a growing interest in underwater acoustic telemetry. Digital underwater communications and networking are becoming increasingly important, with numerous applications emerging in environmental monitoring, exploration of the oceans, and military missions. In contrast to terrestrial radio communications, acoustic communications still rely on extensive field experiments for evaluation of physical-layer algorithms. There is thus an increasing need for acoustic channel simulators and definition of standard test channels. With a growing literature [1, 2] on modulation schemes and their performance in a particular environment, there is still a lack of methods to compare such schemes for realistic underwater channels. By contrast, papers published in the rapidly emerging field of underwater communication networks often compare several network protocols by simulation, e.g. [3].

In order to construct a realistic acoustic channel model or simulator, knowledge of the channel physics and statistics is required. Channel simulation based entirely on acoustic modeling is highly ambitious, and in practice one requires *in situ* channel soundings, i.e., measurements of the time-varying impulse response, to validate models or to drive channel replay simulators [4, 5]. Channel characterization, sounding in particular, is at the basis of realistic channel models and improves understanding of system performance at sea. Existing characterizations investigate miscellaneous aspects of acoustic channels, e.g. [6, 7, 8, 9, 10, 11, 12, 13].

This report describes the technique of channel sounding, basic signal processing, and computation of channel parameters. The relevance for communication systems is evident throughout this report, but channel sounding can also be used just to study the physics of propagation. Techniques are generally applicable to propagation channels, whether it concerns underwater channels, radio channels, or otherwise. Parts of the description are possibly more relevant to the underwater environment, such as correction for time-varying Doppler shifts, delay-Doppler coupling, and aliasing in both delay and frequency. A section with example soundings illustrates the diversity of shallow-water channels and a number of intriguing propagation phenomena.

2 The acoustic channel

The underwater acoustic channel is quite possibly nature's most unforgiving wireless communication medium [14]. Absorption at high frequencies, and ship noise at low frequencies, limit the usable bandwidth to between, say, a few kilohertz and several tens of kilohertz, depending on the range. Horizontal underwater channels are prone to multipath propagation due to refraction, reflection and scattering. The sound speed $c \approx 1.5$ km/s is low compared with the speed of light and may lead to channel delay spreads of tens or hundreds of milliseconds. In certain environments reverberation can be heard ringing for seconds and ultimately limits the performance of communication systems. The low speed of sound is also at the origin of significant Doppler effects, which can be subdivided in time-varying frequency shifts and momentaneous frequency spreading due to various mechanisms. Both phenomena contribute to the Doppler variance of received communication signals, but require

different measures at the receiver. A channel that disperses the signal power in both delay and frequency is known as a doubly spread channel.

Signal fluctuations due to changes within the propagation medium, as opposed to transceiver motion, occur on various time scales [15]. Seasonal, diurnal, and tidal cycles may significantly alter the sound speed profile, and thereby the channel impulse response and propagation loss, but their time scales are very long compared with the duration of a typical communication packet. Such cycles are associated with seasonal (diurnal, tidal) performance variations of communication systems, but not with Doppler spreading and channel tracking at the physical layer. The main cause of frequency spreading that challenges acoustic communication receivers has to be scattering of sound by wind-generated waves [16, 17, 18, 12], where "main cause" refers to both frequency of occurrence and magnitude of the effect. In addition, clouds of air bubbles may form under the surface in the presence of breaking waves [19, 20]. Bubbles scatter and absorb sound, and may also modify the sound speed profile in the top few meters of the water column, thereby enhancing scattering by waves [21]. Other causes of time variability are as diverse as swell, wakes of passing ships, fish shoals, bubble screens due to rain showers, internal waves, a fresh-water front due to river discharge ... the list is long. Currents affect the acoustic wavelength rather than the frequency and do not lead to Doppler shifts, unless they are (rapidly) time varying.

The variety of shallow-water communication channels renders it difficult to design physical-layer solutions that are robust to geographical area, weather conditions, and season. For the same reason it is challenging to design a channel simulator that faithfully mimics all environments, or even to find the most appropriate measurement scheme for *in-situ* soundings. The following, presumably incomplete overview sketches the diversity of channels that can be encountered. The channel may be characterized by correlated or uncorrelated scattering, by (quasi)stationary, cyclostationary, or non-stationary scattering. Shallow-water propagation channels range from stable monopath propagation to overspread, and from sparse to densely populated impulse responses. The most energetic arrival

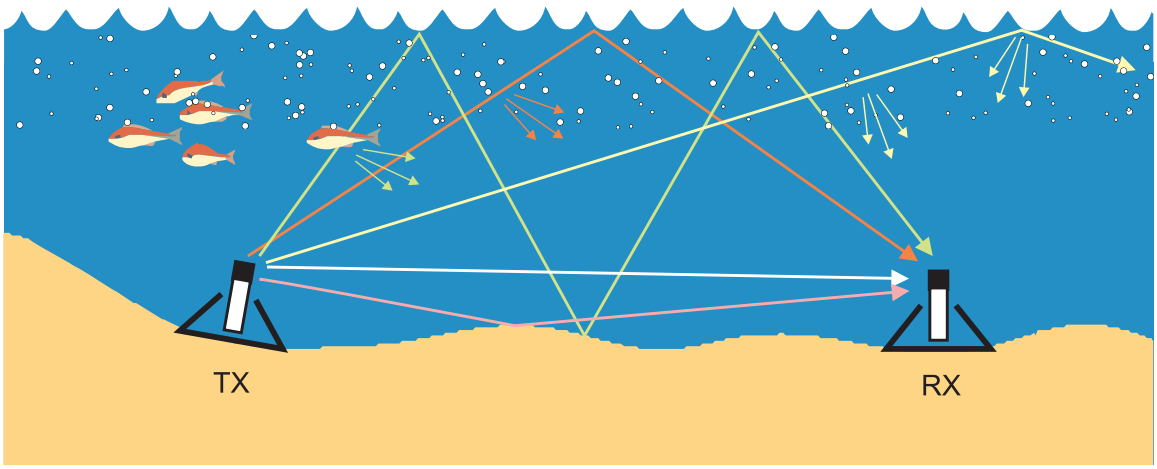

Figure 2.1 Depiction of a shallow-water channel with reflection and scatterers.

may be at the start of the impulse response, at the very end, or somewhere in between. Doppler power spectra range from heavy-tailed to Gaussian, are symmetrical or asymmetrical, centered on zero frequency shift or offset. The Doppler spread may be essentially the same for all paths, for instance for signaling through a sound channel, or vary by orders of magnitude in channels featuring a mixture of specular and surface-reflected paths. Some channels may be characterized as being deterministic, while other ones exhibit Rayleigh, Rician, or K-distributed fading [22]. Section 5 illustrates many of the channel properties mentioned in this paragraph with example shallow-water soundings.

In addition to signal propagation comes ambient noise, from many and varied sources [23]. Noise can be colored and Gaussian when dominated by breaking waves, or impulsive and white when dominated by snapping shrimp or cavitating ship propellers. There are many noise sources with different properties, such as precipitation, marine mammals, cracking ice, sonar systems, offshore construction, platform self-noise. Underwater communication systems are often not limited by noise but by the channel itself. That is, the receiver output signal-to-interference-plus-noise ratio (SINR) is well below the input signal-to-noise ratio (SNR) and text-book bit-error-ratio (BER) curves are inapplicable. Channel estimation errors introduce an effective noise term at the receiver output that reflects self-interference, and this term may be much larger than the true noise term. In that case the noise characteristics are of secondary importance. Whenever an acoustic communication system becomes noise limited, the noise characteristics are obviously important. This report does not deal with noise, but focuses on channel sounding.

3 Probe signals

3.1 PRBS and LFM waveforms

Channel sounding requires transmission of judiciously selected probe signals. The choice depends on channel characteristics, which may or may not be known in advance, the type of signal processing for channel estimation, and properties of the probe signal itself. This report mainly focuses on channel estimation by replica correlation and considers two probe signals that have properties in common but also with differences. These are pseudorandom binary sequences (PRBSs) and linear frequency-modulated (LFM) chirp trains. Hyperbolic frequency-modulated chirps, a popular choice for detection applications, are deemed less suitable for channel sounding [24].

A PRBS is a repetition of a maximal-length bit sequence $c_m \in \{-1, 1\}$, modulated onto a binary phase-shift keyed waveform. The cyclic autocorrelation function of a maximal-length sequence with length M has a zero-lag value of M, and -1 elsewhere. The autocorrelation function is no different for a train of LFM chirps, but in both cases the nice autocorrelation properties only apply to static channels. Doppler effects degrade these properties. With f_c denoting the center frequency, B the bandwidth, T the duration, and $u(t)$ the bit pulse shape, a single "ping" is given by

$$p(t) = \sin(2\pi f_c t) \sum_{m=0}^{M-1} c_m \, u\left(t - \frac{m}{M}T\right) \ , \tag{3.1}$$

$$p(t) = \sin\left(2\pi\left[\left(f_\mathrm{c} - \frac{B}{2}\right)t + \frac{B}{2T}t^2\right]\right) \ , \tag{3.2}$$

for the PRBS and LFM, respectively. In both cases the channel probe signal is constructed as a seamless concatenation of N pings

$$s(t) = \sum_{n=0}^{N-1} p(t - nT) \ . \tag{3.3}$$

The pings are transmitted head to tail, without any pause in between, which is especially important for the PRBS. The LFM ping duration should be chosen such that it covers an integer number of carrier cycles.

3.2 Spectrum

When the sounding is performed with the intention to create archive files for channel simulators operating in replay mode [4, 5], the preferred spectrum of the waveforms is wideband and flatband. Frequencies not covered by the probe signal cannot be simulated. Simply put, if a replay simulator filters a $B = 8$ kHz (communication) signal with a channel obtained from a $B = 5$ kHz probe signal, the filtered signal loses 3 kHz of bandwidth. If the probe signal has a flat spectrum over a frequency interval B, the measured channel can be used without further adaptation to filter communication waveforms with a bandwidth $\leq B$. If the spectrum of the probe signal is not flat its envelope must be deconvolved out of the channel estimate, which leads to noise amplification. Examples of suitable signals are PRBSs using a root-raised-cosine spectrum with a small roll-off factor, and unweighted chirps. For applications where sidelobes in delay are undesirable, frequency weighting can be applied. This can be done at the transmitter but also at reception, leaving the weighting option open. Transfer functions of equipment also affect channel soundings, but here it can be argued that spectral compensation is not required if the same instruments, e.g. acoustic modems, are also employed for communications.

Sections 3.3 and 4.2 show processing examples for PRBS and LFM probes using $f_\mathrm{c} = 14$ kHz. The PRBS is constructed with a bit rate of 8000 bps and a root-raised-cosine spectrum with roll-off factor 1/8. This yields a flat spectrum between 10.5 and 17.5 kHz and a smooth roll-off towards 9.5 and 18.5 kHz. The LFM spectrum is weighted with the same root-raised-cosine shape, such that the PRBS and the LFM waveforms have precisely the same spectral envelope and a -3 dB bandwidth of $B = 8$ kHz between 10 and 18 kHz. The tracking period T is varied to tune the delay-Doppler observation window $T \times T^{-1}$ to different channels. These probe signal parameters also apply to all soundings in Sec. 5 that use a carrier frequency of 14 kHz.

3.3 Ambiguity function

The PRBS and LFM ping types are characterized by their ambiguity functions [25, 26] in Fig. 3.1. These plots give the correlation filter response, for a single ping, as a function of time delay and frequency shift (quantified for the center frequency). A constant Doppler *shift* v is applied to the signal, which differs from the Doppler *spread* channels considered later.

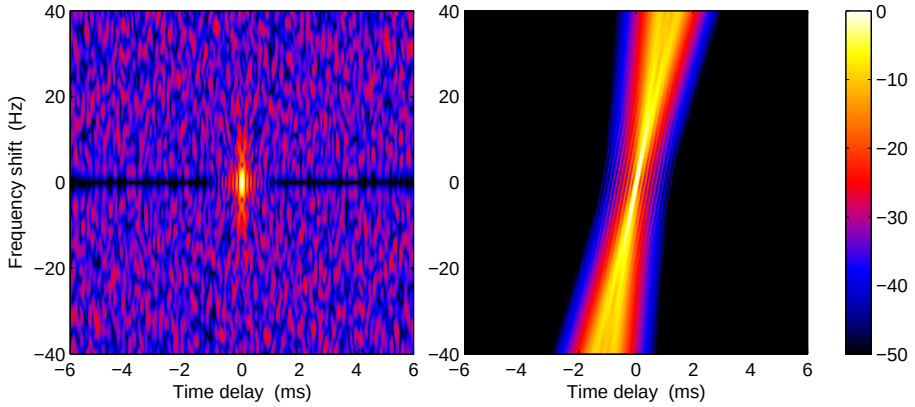

Figure 3.1 PRBS and LFM ambiguity functions, using $T = 256\ ms$.

At zero frequency shift the response is the same for the PRBS and LFM, provided that the PRBS ping is embedded in its cyclic structure. However, elsewhere the surfaces are very different. The PRBS offers a high resolution in both delay and Doppler, but suffers from clutter at $\upsilon \neq 0$. The chirp has a tilted function. It has a much stronger response (peak filter output) than the PRBS for Doppler-shifted signals, but this Doppler insensitivity comes with a delay shift of $\Delta\tau = \upsilon \times T/B$. This phenomenon is known as delay-Doppler coupling, or range-Doppler coupling in ranging applications. The LFM additionally shows some broadening for large frequency shifts.

4 Channel sounding

4.1 Time-varying impulse response

The key objective of channel sounding is to measure/estimate the channel impulse response $h(\tau, t)$ as a function of time delay τ and time t. Once an estimate of $h(\tau, t)$ is available, channel parameters can be derived. To obtain a discrete-time estimate with the probe signals described in Sec. 3.1, a recorded signal is brought to complex baseband, (down)sampled at a rate f_s, and filtered with a baseband replica of the transmit ping. This filter is known as a matched filter or correlation filter. Individual impulse responses are cropped from the long filter output and stacked, so as to obtain a matrix of N complex impulse responses

$$h = h(q, n) \tag{4.1}$$

with corresponding time delays $\tau(q) = q/f_s$ and time instants $t(n) = nT$. The pulse shape of h has a spectrum that is the square of the spectrum of the probe signal. A root raised cosine becomes a full raised cosine. Accurate stacking requires an integer number of samples per ping, and is simply implemented in Matlab by the reshape command. Abundant literature is available on other channel estimation algorithms, which may work on very different waveforms. They differ in the method to obtain $h(\tau, t)$, and may yield different kinds of estimation errors, i.e., departures of the measured $h(\tau, t)$ from the true channel. Apart from these differences, all further processing is the same.

4.2 Delay-Doppler spread

A discrete Fourier transform of h with respect to n gives the spreading function

$$S(q,k) = F(h) = \sum_{n=0}^{N-1} h(q,n) \exp\left(\frac{-2\pi \mathrm{i} nk}{N}\right) , \tag{4.2}$$

where $k \in \left[-\frac{N}{2}, -\frac{N}{2}+1, ..., \frac{N}{2}-1\right]$ corresponds to frequency shifts $\upsilon(k) = k/(NT)$. Physical units are absent in this discrete-time representation; $|S(q,k)|^2$ is a two-dimensional density that gives the relative distribution of signal power, or energy, over the delay-Doppler plane. A stochastic version known as the scattering function can be obtained by taking the expectation of the spreading function. Scattering functions are meaningful in the context of wide-sense stationary uncorrelated scattering (WSSUS) [27]. Examples in this report use the spreading function, which can be considered as a single realization of the scattering function, if indeed the channel is stationary. Spreading and scattering functions are channel properties and differ from the ambiguity function, which is a property of the waveform.

Summation over delay yields an estimate of the Doppler power spectrum

$$P_\upsilon(k) = \sum_{q=0}^{Q-1} |S(q,k)|^2 , \tag{4.3}$$

where $Q = f_\mathrm{s} T$, and summation over the frequency shift an estimate of the power delay profile

$$P_\tau(q) = \sum_{k=0}^{N-1} |S(q,k)|^2 . \tag{4.4}$$

The Doppler spectrum is a power spectral density that characterizes the distribution of received signal power as a function of frequency shift. The power delay profile gives the power distribution over time delay. Units are missing; this report shows dimensionless normalized spectra and profiles.

Since their ambiguity functions are the same at $\upsilon = 0$, PRBS and LFM probes yield the same estimate of the power delay profile in static channels. This is illustrated in Fig. 4.1. The figure shows the power delay profile estimate for a synthetic channel with $L = 6$ multipath arrivals, spaced by 4 ms, whose amplitude and phase are time-invariant. Although there is no noise in the simulation, there is a floor in the power delay profile. This is due to the finite sidelobe levels of the probe signal autocorrelation function. The floor level is obtained from the time-bandwidth product of a ping, or equivalently the m-sequence gain M: $-20\log_{10}((M+1-L)/L) = -32.4$ dB.

The behavior of the PRBS and LFM probes in a rapidly time-varying channel is illustrated in Fig. 4.2. Fading multipath arrivals are mimicked by a tapped delay line with six arrivals, each with a Gaussian Doppler power spectrum characterized by a Doppler spread of 2σ. The spacing between the arrivals is 4 ms, and they still have the same power density, i.e., amplitude in the true power delay profile. When the product of Doppler spread and probe period T becomes of order 1, there is channel variability within a ping and the path amplitude drops. This drop is the same for the PRBS and LFM, but otherwise the power delay profiles are very different. Although Fig. 3.1 shows

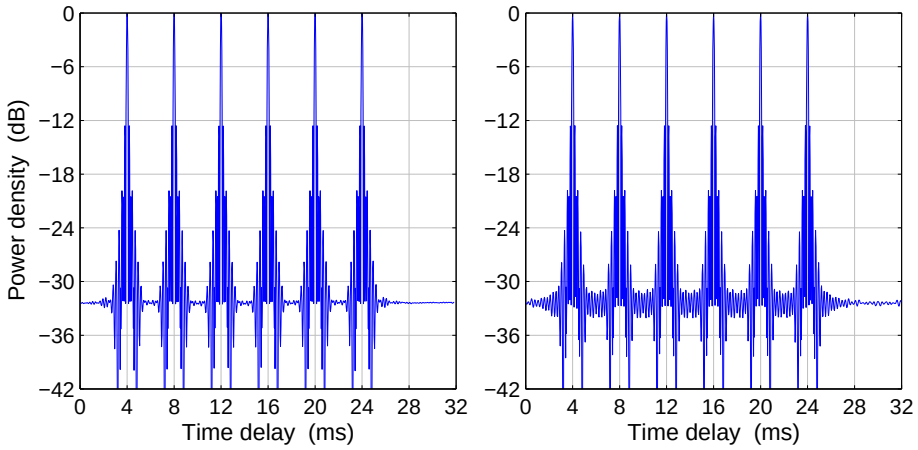

Figure 4.1 *Normalized power delay profiles obtained with PRBS (left) and LFM (right) probes for a static channel. The illustration uses T = 32 ms probe signals.*

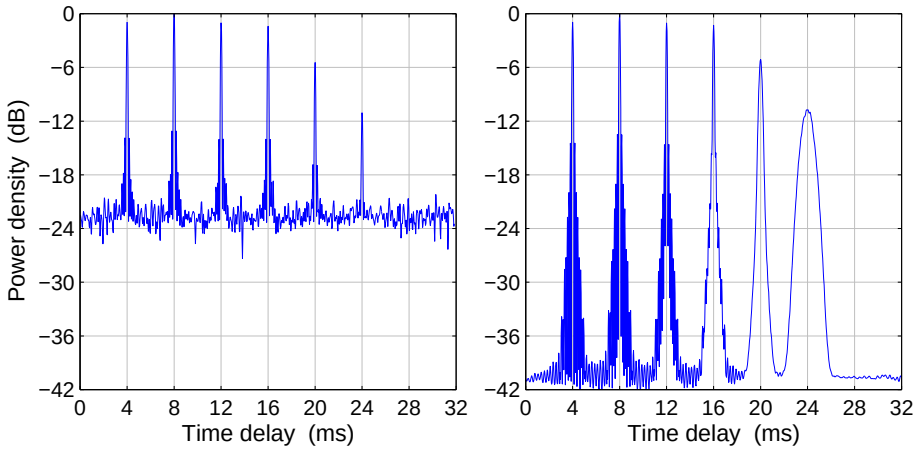

Figure 4.2 *Power delay profiles obtained with PRBS (left) and LFM (right) probes for a channel with 2σ = 0, 1, 4, 16, 64, 256 Hz and a 4-ms path spacing. The illustration uses T = 32 ms probe signals.*

the correlation filter response at a constant frequency shift, it qualitatively explains why PRBS and LFM probes respond differently when there are amplitude and phase fluctuations between pings and within a ping. The measured spreading function is a convolution of the true spreading function and the waveform ambiguity function. Rapid fading causes signal energy to be uniformly scattered in delay for the PRBS. The energy scatter is more localized for the LFM and broadens the fading arrivals. The choice of probe signal thus depends on what is considered more harmful, a loss of resolution in delay (chirp) or an increased interference-plus-noise floor (PRBS). It is presently not clear why the floor has become lower for the LFM probe, compared with Fig. 4.1.

4.3 Aliasing

The period T must be at least as long as the channel delay spread in order to cover the entire impulse response, and the probe rate T^{-1} must be high enough to track the time variability. When the product of delay spread and Doppler spread, known as the channel spread factor, exceeds unity, these demands cannot be met simultaneously and the channel is said to be overspread. Overspread channels unavoidably introduce estimation errors, such as aliasing with cyclic probes. Aliasing may also occur in underspread channels if T is improperly tuned to the channel.

When the tracking period T is too short, the impulse response is aliased in delay and multipath arrivals spaced by T in the true impulse response add up at tap positions $\mathrm{mod}(\tau, T)$ in the processing. This is called temporal aliasing in this report. On the other hand, when the channel fading processes contain frequency components larger than $1/(2T)$, aliasing occurs in the frequency domain. This form of aliasing is sometimes referred to as temporal aliasing, but to avoid confusion with aliasing in delay it will be called spectral aliasing in this report. It is in the frequency domain that aliases appear, anyway. A doubly aliased measurement can be expressed via the spreading function as

$$\tilde{S}(q,k) = \sum_{j=0}^{J_\tau} \sum_{j'=-J_\upsilon}^{J_\upsilon} S(q+jQ, k+j'N) \ , \tag{4.5}$$

where j runs over as many additional intervals $J_\tau \geq 0$ as needed to collect all time-delayed signal energy, and j' over as many additional intervals $2J_\upsilon$ as needed to collect all frequency-spread energy. Time delay lacks a clear origin, unless the travel time from sender to receiver is precisely known, and the index j can be chosen to assume only positive values. There is a minimum travel time from sender to receiver, corresponding to a start of the received signal. Doppler spectra tend to be (near) symmetrical around zero frequency shift, and the index j' naturally assumes positive and negative values. Unlike the power delay profile, the Doppler spectrum has a clear origin.

4.3.1 Overspread channels

It is possible to get rid of temporal or spectral aliasing by tuning T, but not simultaneously if the channel is overspread. If one is only interested in the Doppler spectrum, a sufficiently short T ensures $J_\upsilon = 0$. The measured Doppler spectrum becomes

$$\begin{aligned} \tilde{P}_\upsilon(k) &= \sum_{q=0}^{Q-1} \left| \tilde{S}(q,k) \right|^2 \\ &= \sum_{q=0}^{Q-1} \left| \sum_{j=0}^{J_\tau} S(q+jQ,k) \right|^2 \ , \end{aligned} \tag{4.6}$$

which is not necessarily equal to the spectrum

$$P_\upsilon(k) = \sum_{q=0}^{(J_\tau+1)Q-1} |S(q,k)|^2 \tag{4.7}$$

derived from the true spreading function. In sparse channels there is a low probability of multipath overlap in the presence of temporal aliasing, and $\tilde{P}_\upsilon$ will likely be correct. The same holds for uncorrelated scattering, as the power spectrum of a sum of uncorrelated processes equals the sum of the individual spectra.

On the other hand, if the interest is in the power delay profile a sufficiently long T ensures $J_\tau = 0$. Aliasing occurs in the Doppler spectrum and the properties of the probe signal enter the equation. Spectral aliasing implies channel variations within a ping, and PRBSs and LFMs will distort the power delay profile as illustrated by Fig. 4.2.

The Doppler spread, due to reflection off moving scatterers and relative TX/RX motion, is normally well controlled in the sense that the velocities of the involved scatterers are bounded. This is different for the delay spread. Underwater environments may lead to channels that are characterized by a long reverberation tail, lasting hundreds of milliseconds. This reverberation is due to a three-dimensional scattering volume involving the seafloor, sea surface, and scatterers within the water column. The reverberation level decreases steadily with time delay, perceptibility ending only when it falls below the noise level. Temporal aliasing is unavoidable in such channels, if there is also Doppler to track, deceivingly lifting the noise floor in the power delay profile. Regardless of which form of aliasing is considered, and depending on the application, the channel sounding may still be useful if the aliased power is a sufficiently small fraction of the total.

4.3.2 Temporal aliasing

Figure 4.3 illustrates temporal aliasing. A stationary acoustic channel was probed with $T = 128$ ms and $T = 16$ ms waveforms. The resulting power delay profiles are normalized and synchronized so as to peak at $\tau = 0$. The 128-ms measurement captures most of the time-dispersed power, but not 100% as there is still a decaying reverberation level at the end of the observation window. Notice that the measurement is cyclic, and the portion shown before $\tau = 0$ is the continuation of the tail at the right of the graph. The 16-ms probe covers too short a delay interval, and aliasing is observed. First, the distinct arrivals at $\tau = 19$ and $\tau = 22$ ms in the 128-ms profile falsely appear at $\tau = 3$ and $\tau = 6$ ms in the 16-ms data. Second, the long reverberation tail is multiply aliased and lifts the noise floor, filling gaps where the true profile has a low power density. Although the reverberation level is below –16 dB everywhere, the continuum of signal power density has a non-negligible integral. This is corroborated by the green curve in Fig. 4.3. This profile is obtained by assuming the 128-ms spreading function to be the true spreading function. An artificially aliased profile is computed via Eq. 4.5, using $J_\tau = 7$ and $J_\upsilon = 0$. The green profile is not separately normalized, but follows directly from the 128-ms data. There is a fairly good agreement between the measured and simulated 16-ms profiles. The huge increase of the interference-plus-noise floor is mostly accounted for by the aliased power, and perhaps for a small part by the lower processing gain of the $T = 16$ ms waveform.

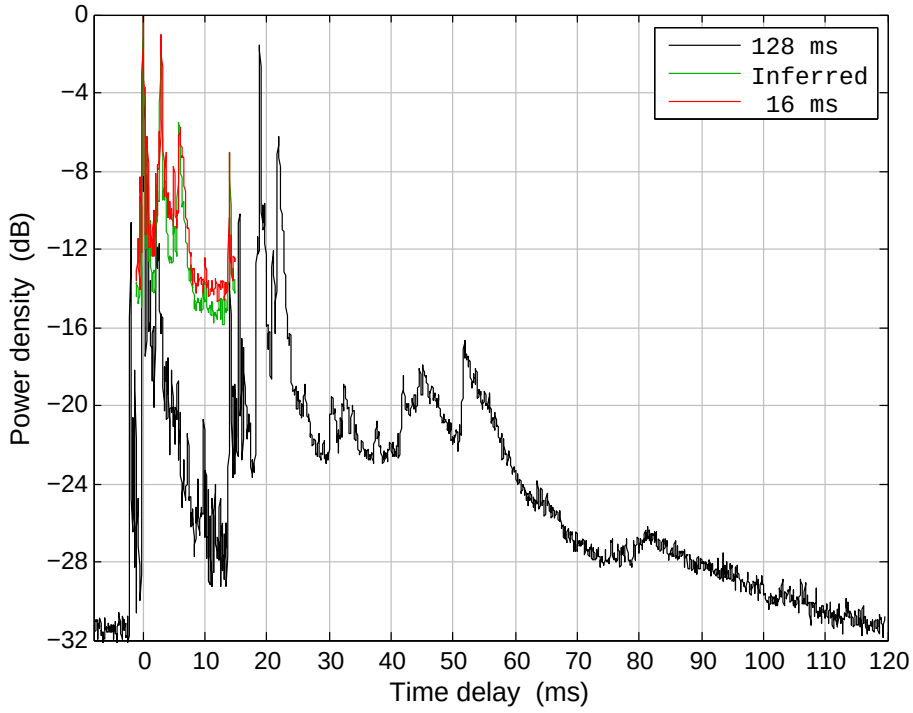

Figure 4.3 Temporal aliasing: measured power delay profiles for $T = 128$ and 16 ms.

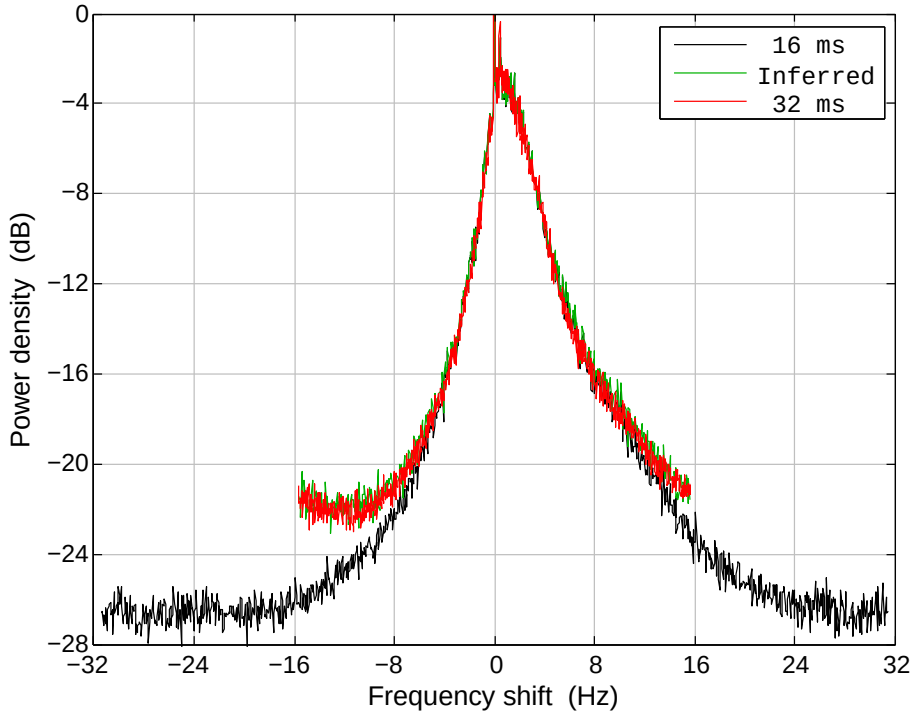

Figure 4.4 Demonstration of spectral aliasing. Doppler spectra are shown for two probe signals, using $T = 16$ and 32 ms.

4.3.3 Spectral aliasing

Spectral aliasing is shown in Fig. 4.4. A stationary acoustic channel was probed with $T = 16$ ms and $T = 32$ ms waveforms. The 16-ms probe has a wide Doppler observation window and captures the entire spectrum before it disappears below the noise floor. The 32-ms spectrum is identical to the 16-ms spectrum down to –16 dB, but deviates at its boundaries. In this particular case the Doppler spectrum is not symmetrical about $v = 0$, and aliasing manifests itself notably with an upward bend at the left side of the 32-ms spectrum. Energy that falls out at the right side enters at the left side, and vice versa. The green spectrum is obtained by assuming the 16-ms spreading function to be the true spreading function. An artificially aliased spectrum is computed via Eq. 4.5, using $J_\tau = 0$, $J_v = 1$, and zero padding to obtain the required number of samples. The similarity of the green and red curves provides agreement between theory and practice, simultaneously supporting the claim of channel stationarity between the 16-ms and 32-ms measurements.

4.3.4 LMS channel estimation

Aliasing is a drawback of the cyclic structure of PRBSs or chirp ping trains, and can be avoided by using different waveforms and channel estimation algorithms. For example, a random phase-shift keyed symbol stream combined with the least mean squares (LMS) algorithm. Such a scheme allows channel updates at the symbol rate and has no limitation in time delay. Moreover, there is no need to decide on the tracking period T before sea experiments. However, there exists a trade-off between channel length and tracking capability and there will be estimation errors. It is not expected

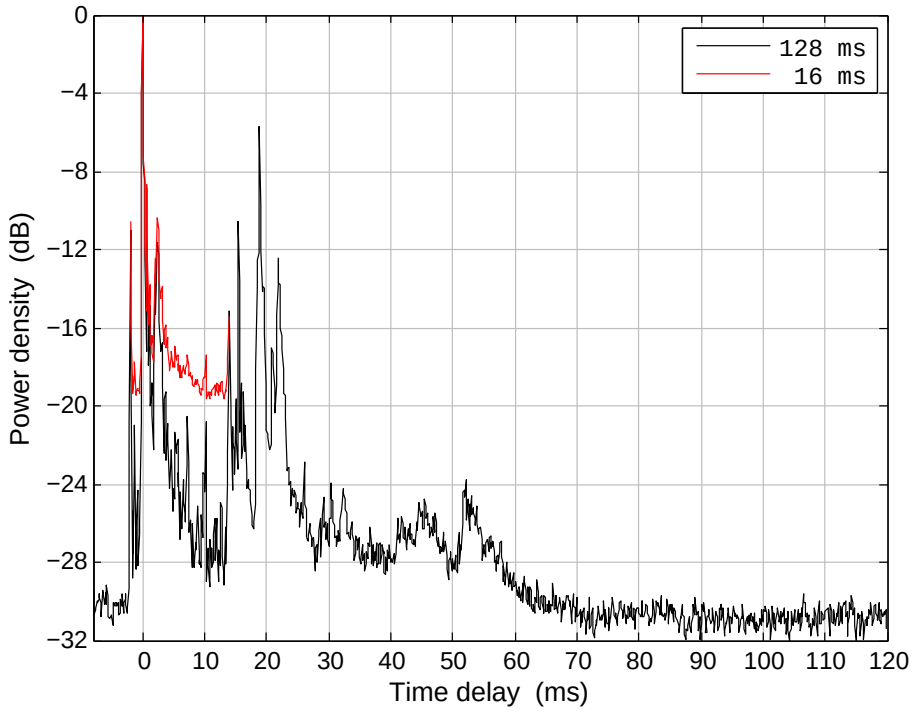

Figure 4.5 Power delay profile estimates obtained by LMS channel estimation.

that alternative estimation methods will generally outperform the matched-filter estimator, but they may improve upon certain aspects such as aliasing.

Figure 4.5 illustrates this with power delay profiles obtained by LMS channel estimation. The algorithm is applied to a BPSK modulated random bit stream at 8000 bps that was transmitted in tandem with the probe signals of Fig. 4.3. Signal spectrum and SNR are the same. For comparison with the matched-filter estimates in Fig. 4.3 the estimation is performed with two channel vector lengths, corresponding to delay intervals of 128 and 16 ms. Note that the profiles in Fig. 4.5 are obtained from a single waveform, whereas the profiles in Fig. 4.3 come from two separate signals.

The 128-ms LMS estimate resembles the matched-filter result, but underestimates the power density of the delayed arrivals and the reverberation tail. In this case the reverberation originates from surface scattering, and is thus time varying. With the large number of channel taps required for a 128-ms delay coverage, the convergence time of the algorithm is too long to track rapid time variations. LMS channel estimation has difficulty with such channels, a conclusion that is based on more data than the single comparison between Fig. 4.3 and Fig. 4.5. LMS Doppler spectra tend to be narrower than their correlation-estimator counterparts. On the other hand, the 16-ms LMS estimate in Fig. 4.5 is more clean than its counterpart in Fig. 4.3 as there is no aliasing, but there is still an effective noise floor. Arrivals outside the extent of the channel vector act as noise. The LMS estimate for the 16-ms interval is better than in Fig. 4.3 whereas the 128-ms LMS profile is worse. Obviously a 16-ms profile misses a large part of the impulse response, and the 128-ms matched-filter profile is the best overall result. A detailed comparison between the correlation estimator and other methods is beyond the scope of this report. All soundings in Sec. 5 use the correlation estimator.

4.4 Time-varying Doppler shifts

The WSSUS assumption does not always apply to underwater acoustic channels. There are many possible reasons, but one of the most prominent causes is TX/RX motion. When the transmitter and receiver move relative to each other, the signal experiences time compression or dilation. This manifests itself as a time-varying travel time and a twofold violation of WSSUS. The time dilation is to a large extent the same for all propagation paths, depending on the geometry, and introduces correlation in range rate and phase. Non-zero range rates cause multipath arrivals to drift between taps, in a tapped-delay-line representation, resulting in channel non-stationarity. Channel soundings reveal a smearing of the power delay profile and a broadening of the Doppler spectrum, even if the propagation medium itself is time-invariant.

The Doppler variance can receive significant contributions from TX/RX motion even if modems are deployed from an anchored ship or gateway buoy. Channel soundings meant to study the propagation medium itself require senders and transmitters in a frame on the seafloor, fixed to a quay, or similar. This is not always feasible, and the next best thing is to remove time-varying Doppler shifts (TVD) from the data by resampling operations. Fig. 4.6 shows an iterative procedure culminating in the elimination of kinematic effects from the measured impulse response $h(q, n)$. The first step is the removal of a constant velocity v_0 by resampling the received signal with a

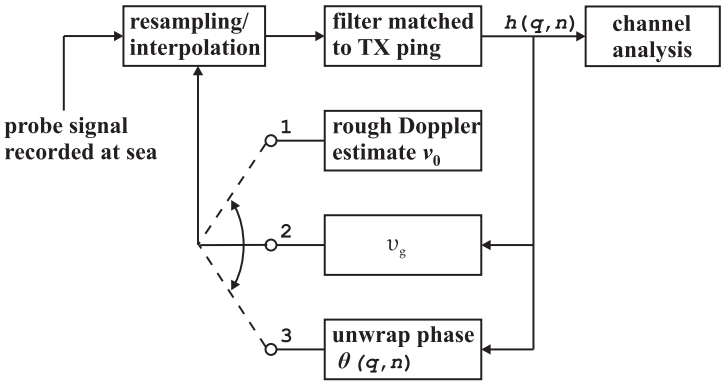

Figure 4.6 Iterative procedure to eliminate constant and time-variable Doppler shifts from the sounding $h(q, n)$.

resampling factor $1 - v_0/c$ prior to the matched filter, where $c = 1500$ m/s is the nominal speed of sound and the sign convention for v_0 such that a positive velocity corresponds to an increasing range. The value of v_0 can be a rough guess, an automated estimate obtained with a bank of Doppler-shifted ping replicas, where a PRBS has an advantage over chirps, or be the result of a brute-force search. In the case of a stationary set-up it may be derived from known clock-frequency offsets, which result in apparent Doppler shifts. Its accuracy must be such that the bulk of the spectrum falls in the $[-1/(2T), (1/2T)]$ regime after resampling. The next step is fine adjustment, for instance by shifting the center of gravity

$$v_g = \sum_{k=-N/2}^{N/2-1} \frac{k}{NT} P_v(k) \left(\sum_{k=-N/2}^{N/2-1} P_v(k) \right)^{-1} , \tag{4.8}$$

of the spectrum after the first resampling step, to zero frequency shift. The resampling factor that achieves this is given by $1 - V_0/c$, with

$$V_0 = v_0 - \frac{v_g}{f_c} c \, . \tag{4.9}$$

In case of apparent Doppler shifts due to clock frequency offsets of modem electronics, full correction is possible by resampling with a constant factor. However, the Doppler shift due to movement generally varies with time, which requires a third compensation step to remove TVD around the mean shift. To this end the unwrapped phase $\theta(q_j, n)$ of $h(q_j, n)$ is upsampled from the channel tracking rate to the sampling frequency of the recorded data, and used to drive an interpolator that computes the signal at unevenly spaced times $t' = t - \theta(q_j, t)/(2\pi f_c)$. The overall procedure is equivalent to a time-variable resampling factor

$$R(t) = 1 - \frac{V_0}{c} + \frac{1}{2\pi f_c} \frac{\mathrm{d}\theta(q_j, t)}{\mathrm{d}t} \tag{4.10}$$

applied to the recorded probe signal. A natural choice for $\theta(q_j, t)$ is the phase of the most energetic arrival, although an average over multiple arrivals can also be considered. Notice that the intermediate step 2 in Fig. 4.6 is needed to obtain a good phase measurement for the third

step. Uncompensated Doppler causes multipath arrivals to gradually drift from one tap to the next, compromising the phase measurement for a given tap. In the presence of strong TX/RX acceleration even the condition $v_g = 0$ is insufficient, with multipath arrivals noticeably wandering between taps. See for instance Fig. 5.11. In such cases the third step of Fig. 4.6 may be repeated by accumulating phase measurements of successive iterations.

4.5 Definitions of delay spread and Doppler spread

The impulse response $h(q, n)$ and its Fourier transform $S(q, k)$ are complete descriptions of a measured channel. Derived scattering functions completely characterize the second-order statistics, but only for WSSUS channels. The power delay profile and Doppler spectrum present condensed information and do not allow channel reconstruction, unless it happens to be separable according to $S(q, k) = \sqrt{P_\tau(q)P_v(k)/P}$, with P denoting the total signal power. A further loss of information occurs when the channel is reduced to only two parameters, known as the delay spread and the Doppler spread. These have limited significance and do not allow reconstruction of the power delay profile or Doppler spectrum, let alone the channel itself. An exception occurs when the profile or spectrum has a familiar shape. E.g., a Doppler spread of $2\sigma = 1$ Hz completely describes a Gaussian power spectrum. Unfortunately real spectra are rarely Gaussian. Nonetheless parameterization of Doppler spectra appears to be possible, to some extent: see Sec. 7.

There are many definitions of delay and Doppler spread in circulation. The following definitions are for the delay spread $\mathcal{T}$; the Doppler spread $\mathcal{D}$ is similarly defined from the Doppler power spectrum as the delay spread from the power delay profile. It is assumed that P_τ and P_v are normalized to unity.

The threshold delay spread is the difference between the longest and shortest delay where the profile equals or exceeds a given threshold value X

$$\mathcal{T}_{\text{thr}} = \tau\left(\max_q \{q \mid P_\tau \geq X\}\right) - \tau\left(\min_q \{q \mid P_\tau \geq X\}\right) . \tag{4.11}$$

The RMS delay spread is defined as

$$\mathcal{T}_{\text{rms}} = \left(\sum_{q=0}^{Q-1} P_\tau(q)\left[\tau(q) - \tau_{\text{g}}\right]^2 \left[\sum_{q=0}^{Q-1} P_\tau(q)\right]^{-1}\right)^{1/2} , \tag{4.12}$$

where τ_{g} denotes the center of gravity

$$\tau_{\text{g}} = \sum_{q=0}^{Q-1} \tau(q)P_\tau(q)\left(\sum_{q=0}^{Q-1} P_\tau(q)\right)^{-1} \tag{4.13}$$

of the power delay profile. The threshold and RMS definitions are two commonly used criteria, where RMS is said to be more relevant to the performance of communication systems [28]. A third, less common definition is physically intuitive and uses an energy (power) criterion. The normalized

accumulated power is computed

$$E(q) = \sum_{q'=0}^{q} P_\tau(q') \left(\sum_{q'=0}^{Q-1} P_\tau(q') \right)^{-1} , \tag{4.14}$$

and this function is used to find the border points

$$\max_{q_1} \min_{q_2} \{ q_1, q_2 \mid E(q_2) - E(q_1) \geq \Gamma \} , \tag{4.15}$$

of the shortest possible delay interval that captures a given fraction Γ of the total signal power. The corresponding delay spread $\tau(q_2) - \tau(q_1)$ is denoted $\mathcal{T}_{\text{en}}$.

Note that the definitions are theoretical and that accurate measurement is not always feasible. Values are sensitive to noise and aliasing for all criteria, especially for small X or large Γ. Cyclic delay shifts may additionally affect delay spread values. Channel estimation errors such as in Fig. 4.2 may have a big effect on $\mathcal{T}_{\text{thr}}$, whereas $\mathcal{T}_{\text{rms}}$ and $\mathcal{T}_{\text{en}}$ will be fairly accurate for the LFM probe—but not for the PRBS. When accurate measurement is feasible, the definitions still have their particular strengths and weaknesses. A small change in multipath power can have a large effect on $\mathcal{T}_{\text{thr}}$ by shifting the amplitude of an early or late arrival just above or below the threshold value. $\mathcal{T}_{\text{rms}}$, when used to assess system performance, is overly sensitive to trailing arrivals with little power but a long delay [29]. Figure 4.7 illustrates the treacherous terrain. In this channel the cluster of delayed arrivals has an accumulated power that approximately equals the power of the precursor. There is a thin line between a delay spread of 0 and 400 ms using the -10 dB criterion, whereas a noise floor of -25 dB over such a long stretch is high enough to affect the RMS and energy values. The 50%-energy delay spread obtained from the measured profile amounts to 200 ms, but should be

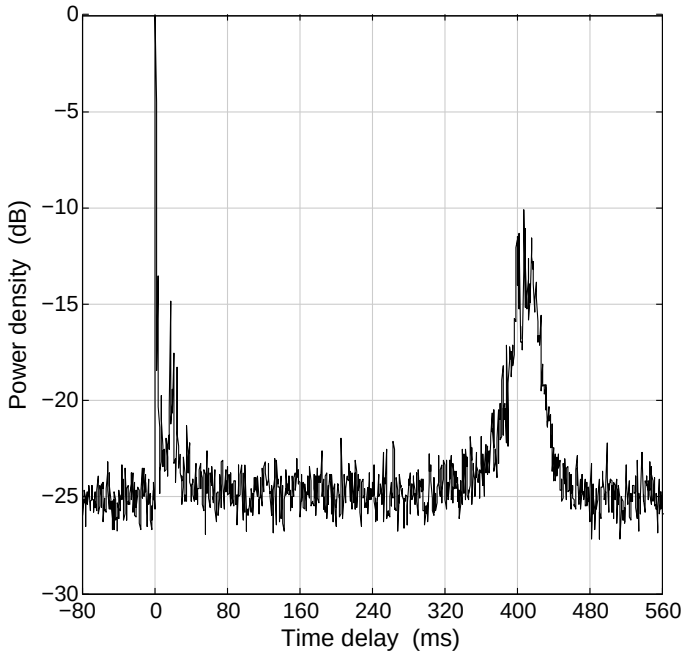

Figure 4.7 Peculiarly sparse power delay profile measured in the Baltic Sea.

much smaller for a noise-free profile. There is no substitute for inspection of a complete profile to see how it relates to the design of a communication scheme.

When the channel spread can be measured accurately, the energy criterion is attractive for system design and performance prediction. In order to be able to achieve a given performance, a receiver needs to have access to a given fraction of the received signal power in delay-Doppler space. Signal energy that is not available, for instance because of a restricted equalizer length, acts as self-interference and lowers the signal-to-interference-plus-noise ratio (SINR).

4.6 Temporal coherence

A time-varying impulse response requires communication receivers to update their channel estimates in order to maintain good performance over time. A measure of the rate at which the channel changes is the coherence time, which is a time interval over which the coherence drops by some specified amount. Temporal coherence is addressed by the channel correlation function $C(\Delta t)$, where $\Delta t = t - t_0 = (n - n_0)T = \Delta nT$ is a time interval relative to a reference time t_0.

In WSSUS theory, the correlation function is the inverse Fourier transform (IFT) of the Doppler power spectrum

$$
\begin{aligned}
C_v(\Delta n) &= F^{-1}\left(P_v(k)\right) && (4.16)\\
&= F^{-1}\left(\sum_{q=0}^{Q-1} S^*(q,k)S(q,k)\right) && (4.17)\\
&= F^{-1}\left(\sum_{q=0}^{Q-1} [F(h(q,\Delta n))]^*[F(h(q,\Delta n))]\right) && (4.18)\\
&= \sum_{q=0}^{Q-1} F^{-1}\left(F\left[\sum_j h^*(q,j)h(q,j+\Delta n)\right]\right) && (4.19)\\
&= \sum_{q=0}^{Q-1}\sum_j h^*(q,j)h(q,j+\Delta n) = C_{\mathrm{a}}(\Delta n)\ , && (4.20)
\end{aligned}
$$

where the step between Eq. 4.18 and Eq. 4.19 uses the Autocorrelation (Wiener Khinchin) theorem. C_{a} is the sum over all taps of the autocorrelation function with respect to t. Another estimate of temporal coherence from a measured channel is the normalized zero-lag cross-correlation with respect to τ

$$
C_{\mathrm{c}}(\Delta n) = \frac{\sum_{q=0}^{Q-1} h^*(q,n_0)h(q,n)}{\sqrt{\sum_{q=0}^{Q-1} h^*(q,n_0)h(q,n_0)\sum_{q=0}^{Q-1} h^*(q,n)h(q,n)}}\ . \qquad (4.21)
$$

The normalization is sometimes desirable and sometimes not. When the channel changes just by a scaling factor, a BPSK or QPSK receiver would not strictly require updates but a system employing

a higher-order constellation would. The zero-lag ingredient is also subject to discussion. When the entire impulse response shifts in delay, such as with time compression/dilation due to transceiver motion, some would say that the channel does not really change. However, an adaptive equalizer senses a change and needs to update its filter coefficients to deal with the delay shift.

The IFT correlation function C_υ, the autocorrelation function C_a, and the cross-correlation function C_c are all estimates and not necessarily the same for measured channels. C_υ and C_a are equivalent on the WSSUS assumption, which requires an infinite observation period (infinite support for j). This condition is not met for *in situ* soundings, but C_υ may be approached by C_a if the latter is obtained via an unbiased estimate. Furthermore, stationarity is assumed and C_υ and C_a yield symmetrical correlation functions independent of t_0. By contrast, C_c does not assume anything about the channel but just evaluates the similarity between successive impulse response measurements and a reference snapshot. It does not need to be symmetrical and may depend on t_0 even in stationary channels. It also suffers from an effective noise floor, because the cross-correlation of two random-noise vectors is not small unless the vectors are large. C_a is the expectation (time average) of C_c, if the normalization in Eq. 4.21 is omitted.

The example channels in the next section are illustrated with a comparison between the cross-correlation coherence C_c and the estimate C_υ obtained from the Doppler spectrum. Agreements and deviations provide clues as to the stationarity of the channel. Especially the presence or absence of Doppler spreading and time dilation due to TX/RX motion will prove to make a big difference.

The coherence time of a channel may be defined as the time over which a normalized correlation function drops from 1 to, say, 0.5, and will be denoted by $\mathcal{C}_{0.5}$. A single coherence time fails to adequately parameterize correlation functions of arbitrary shape, and the example channels of the next section demonstrate that the shape indeed varies considerably between channels.

5 Example channels

This section presents a cross section of channel soundings collected over the past five years. All examples concern horizontal shallow-water channels, the majority from northern European waters. The collection is diverse and illustrates that there is no typical or average acoustic channel.

Thirteen channels are considered, labeled A through M. It is not feasible to describe sounding conditions and environments in detail, but Table 5.1 provides a concise overview. N is the number of pings used for the processed results; the actual number of transmitted pings is $N + 2$. The reason is that the first and last impulse response extracted from a PRBS are no part of its cyclic autocorrelation function. They are stripped off. An important column is the one that says whether the TX/RX deployment was static, with sender and receiver firmly mounted in frames on the seafloor (as in Fig. 2.1) or whether there was relative TX/RX motion. The SNR of the received probe signals is moderate to high, which is exactly what is needed for channel sounding. The purpose is to measure the time-varying impulse response, not noise.

Analysis results are shown in the form of figures with six panels, which show *estimates* of:

- Channel, $|h(q,n)|^2$, Eq. 4.1.
- Spreading function, $|S(q,k)|^2$, Eq. 4.2.
- Doppler spectrum Eq. 4.3.
- Residual phase. This is the unwrapped phase $\theta(q_j, n)$ after resampling (if any). The phase measurement is shown for the main multipath arrivals, those which are within ≈ 10 dB of the strongest path in the power delay profile. The black curve is the phase of the strongest path, weaker arrivals use shades of gray.
- Power delay profile Eq. 4.4.
- Correlation function. The magnitude of the functions $C_v(\Delta n)$ and $C_{\mathrm{c}}(\Delta n)$, Eqs. 4.16 and 4.21. The reference impulse response $h(q, n_0)$ is chosen halfway the probe signal.

All quantities plotted on a logarithmic scale are given in decibels relative to their maximum value. Note that the soundings are *possibly* aliased, such that $\tilde{S}$ is shown instead of S, affecting also the other panels. This varies from case to case. The figures for channels A–M in the following sections use different color maps, so as to best highlight features of interest. For the same reason, the delay and frequency axes frequently zoom in on interesting regions. The summary in Tables 5.2 and 5.3 is always based on the full $T \times T^{-1}$ observation window.

Ch.	TX/RX	Probe	T (ms)	N	f_{c} (kHz)	B (kHz)	Range (km)	Water depth (m)	SNR (dB)	Month
A	Static	LFM	128	256	14	8	0.50	10	52	OCT
B	Static	PRBS	32	1024	14	8	0.75	5–16	29	MAY
C	Static	PRBS	32	1024	14	8	0.75	5–16	35	MAY
D	Static	Var.	Var.	Var.	14	8	1.15	20–80	15	OCT
E	Static	PRBS	32	1024	14	8	0.90	10–70	27	OCT
F	Static	PRBS	32	1024	14	8	0.90	10–70	26	OCT
G	Static	PRBS	32	1024	14	8	1.16	9–17	14	OCT
H	Static	LFM	128	256	14	8	1.16	9–17	31	OCT
I	Moving	PRBS	128	248	5	4	38	60–90	23	AUG
J	Moving	PRBS	128	248	5	4	21	250	11	SEP
K	Moving	PRBS	145	203	3.85	3.5	1.2	400	23	SEP
L	Moving	PRBS	102	290	15	10	1.5	100	30	JUN
M	Moving	PRBS	128	232	6	4	6.7	240	31	FEB

Table 5.1 Summary of experimental details for the example channels.

5.1 Channel A

An exceptionally benign communication channel was encountered in Horten's natural bay. Propagation over 500 m at a 10-m water depth resulted in a spreading function that approaches a double Dirac function. There is a tiny bit of broadening in the delay profile, but only below –30 dB and close to the chief arrival. Similarly, the Doppler spectrum is a spike all the way down to –40 dB. The frequency spread observed below this level is not due to noise, but to small fluctuations in signal amplitude and phase, visible as a ripple in the phase measurement. Possible causes of these fluctuations are channel physics, instrument jitter, transducer vibration by current. However, at -50 dB such sidelobes are hardly important and this channel sustains high-rate communication without any form of channel equalization or tracking. Fig. A.1 reveals the noise floor.

To reveal the narrow Doppler spectrum with long-duration probe signals in a static channel, very precise resampling is necessary. Although the transmitter and receiver are bottom-mounted, there are offsets of their clock frequencies from the nominal value, resulting in an apparent Doppler shift. A value $V_0 = -0.1581$ m/s has been used (see Eq. 4.10) for Fig. 5.1; Fig. A.2 shows the sounding result for $V_0 = -0.16$ m/s. The phase $\theta(\tau = 0, t)$ is now subject to a drift of $(\Delta V_0/c)2\pi f_c NT = -3.7$ radians, enough to distort the Doppler spectrum and IFT correlation function. Total neglect of clock-frequency offsets ($V_0 = 0$) would seriously misrepresent the channel.

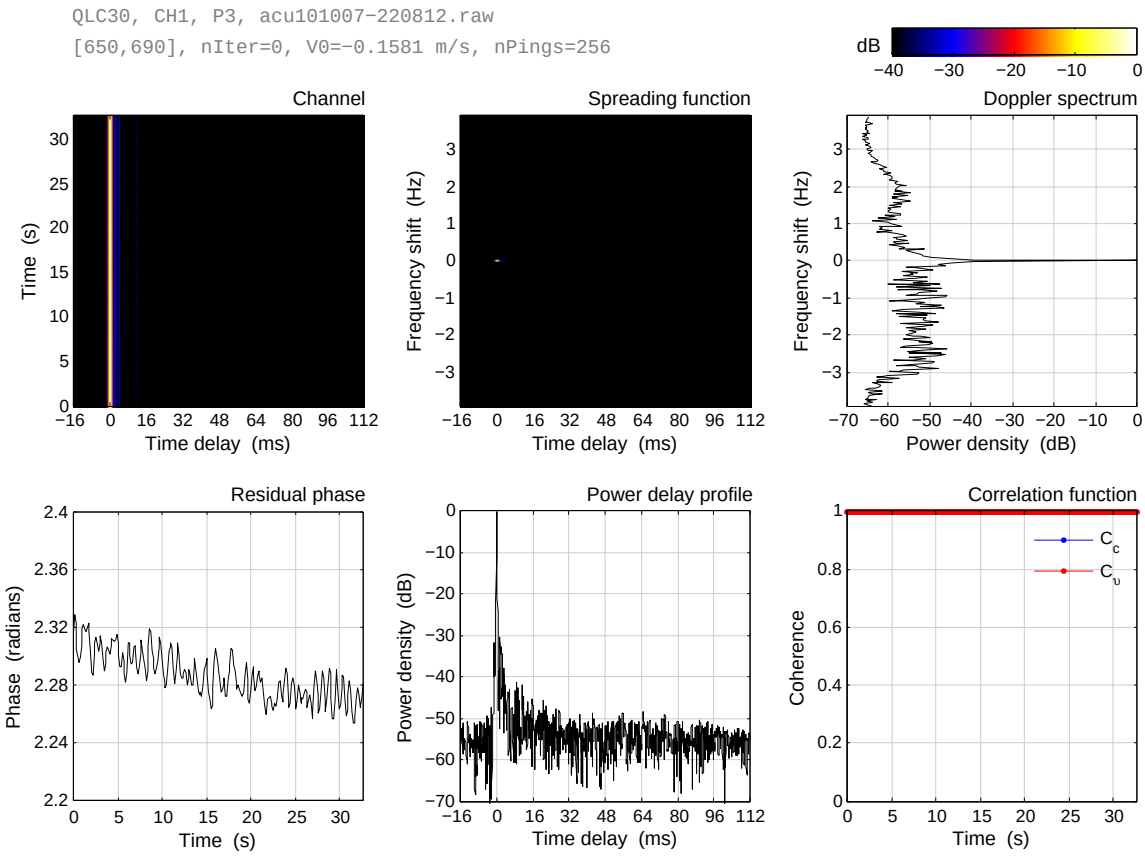

Figure 5.1 Channel A. Benign channel.

5.2 Channel B

Channel B was sounded in the shallow waters of the Bastøyrenna near Horten. There are three closely spaced strong arrivals in the power delay profile that include specular paths, i.e., direct or bottom-reflected paths with negligible amplitude or phase fluctuations. Later arrivals have interacted with the sea surface and are fading. Compared with channel A the specular energy still dominates the Doppler spectrum, but the contribution of fading arrivals is no longer negligible. The Doppler spectrum broadens below -20 dB, and also features sidelobes at a frequency shift that corresponds to the frequency of the most energetic surface gravity waves.

The two correlation functions are the same and immediately tell that the specular paths carry 60% of the received signal power. It takes 0.5 s for $C(\Delta t)$ to drop from 1 to 0.6, and then it remains constant. A coherence time $\mathcal{C}_{0.5}$ makes no sense for this channel and cannot be measured with a 32-s probe signal. If it could be measured with a longer probe signal its value would be very large and misleadingly suggest a nearly static channel. Channel B allows low-rate (spread spectrum) communications without channel tracking, see Sec. 6.2, but a high-rate communication system needs to harvest more than 60% of the signal energy and requires tracking. Note that additive noise can also introduce a spike-like feature in the correlation function [9]; in the present case it is a channel property.

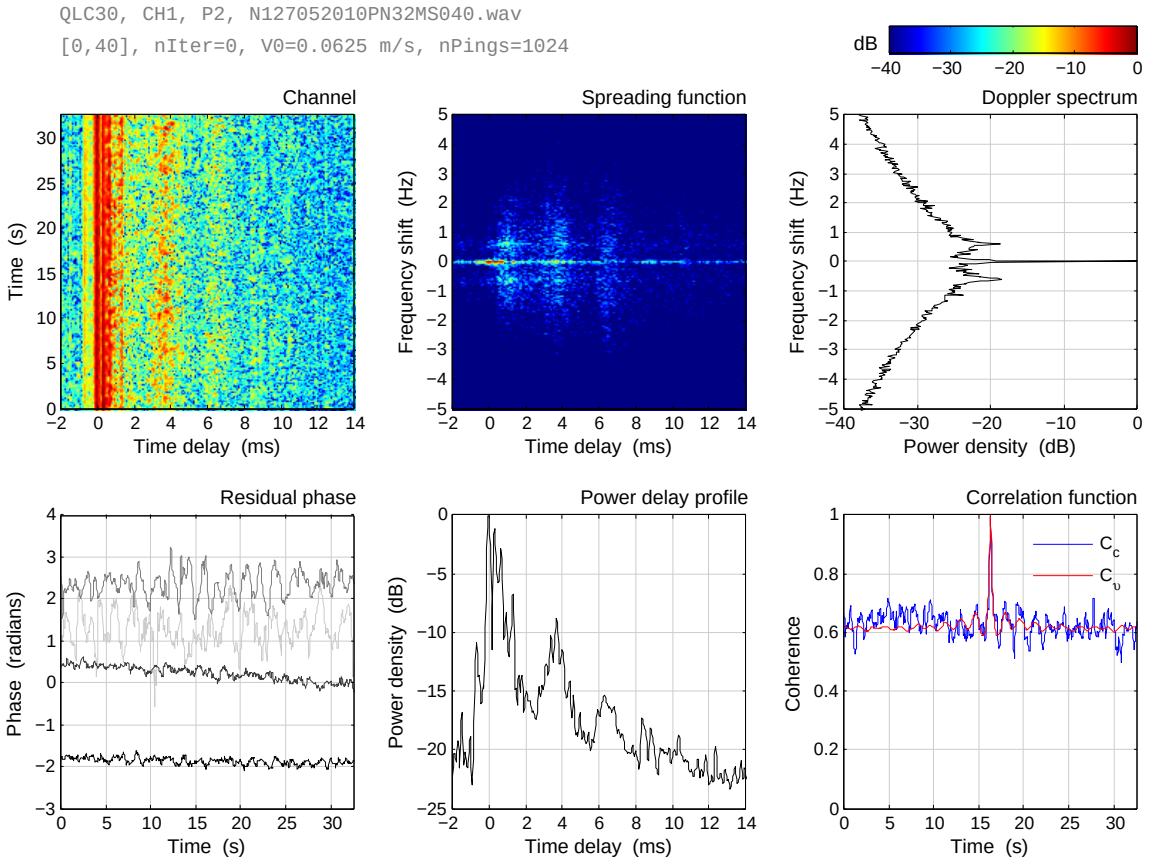

Figure 5.2 Channel B. Stationary channel with a mixture of stable and surface interacting paths.

5.3 Channel C

The geometry and set-up of channel C are the same as those of B, but the sounding took place half a day later and in the presence of a passing ship. Channel properties are very different. Periodicity is observed in both amplitude and phase of different arrivals, and paths are strongly correlated among one another. Fig. A.3 confirms that the uncorrelated scattering of B has become correlated in C. The phase of the specular path at $\tau = 0$ is constant (at -2 radians in the graph), whereas other paths are subject to phase oscillations. The Doppler spectrum features a series of equidistant peaks. This channel has cyclostationary properties over shorter intervals, but is non-stationary when considered over the entire 32-s observation period.

Similar to channel B, the correlation functions do not really drop below 0.5. An alternative criterion such as $\mathcal{C}_{0.8}$, used in [9] to avoid the coherence variance at low values, is ill-defined as the threshold is crossed repeatedly. C_v reproduces the oscillation period of C_c, but is not identical because the statistics change over the 32-s sounding period. The presumable cause of the cyclostationarity is the wake of the passing ship. Ship waves are relatively narrowband and can account for the narrow sidelobes in the Doppler spectrum, which includes higher harmonics, e.g. due to multiple surface bounces. A passing ship is also in agreement with the time scale of the phenomenon as it emerges and disappears, which can be observed with previous and later channel probes.

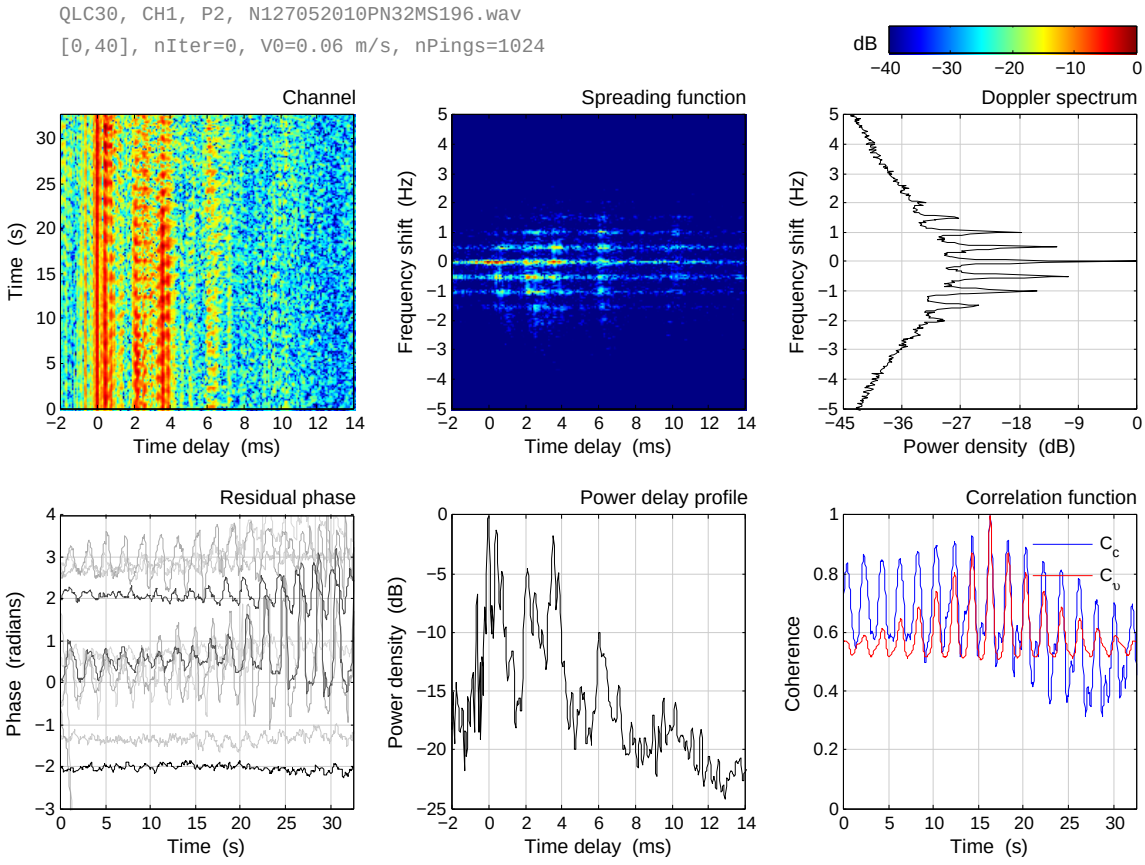

Figure 5.3 Channel C. Non-stationary channel with cyclostationary elements.

5.4 Channel D

Two weeks after the sounding of channel A, soundings were conducted in another part of Norway. The transmitter and receiver were placed in a surface channel created by cooling of the water column at the onset of winter. At a significant wave height of 1 m, the contrast with channel A is enormous. The signal power is everywhere and nowhere at the same time in the (τ, t) plane, with no distinct or dominant arrivals. Figure 5.4 uses a 16-ms PRBS, which captures the full extent of the Doppler power spectrum but not the delay profile. There is considerable aliasing in delay, resulting in a massive floor of self-interference in the estimate of the power delay profile, as explained in Sec. 4.3.2. Channel D proves too difficult for low-rate incoherent and coherent communication schemes operating at 80 bps [30].

The shape of the spectrum approaches a Gaussian, slightly offset from $\upsilon = 0$. It appears to be independent of delay, but because of the aliasing this cannot be stated with certainty. The scattering appears to be totally uncorrelated, and despite the aliasing the overall Doppler spectrum is likely correct. This channel is further illustrated by Fig. A.4, which zooms in on the temporal coherence and uses a different probe to estimate the power delay profile. The correlation function drops rapidly, but on a time scale that is still longer than the tracking period T. The coherence time $\mathcal{C}_{0.5}$ can be measured, and there is excellent agreement between C_{c} and C_{υ}.

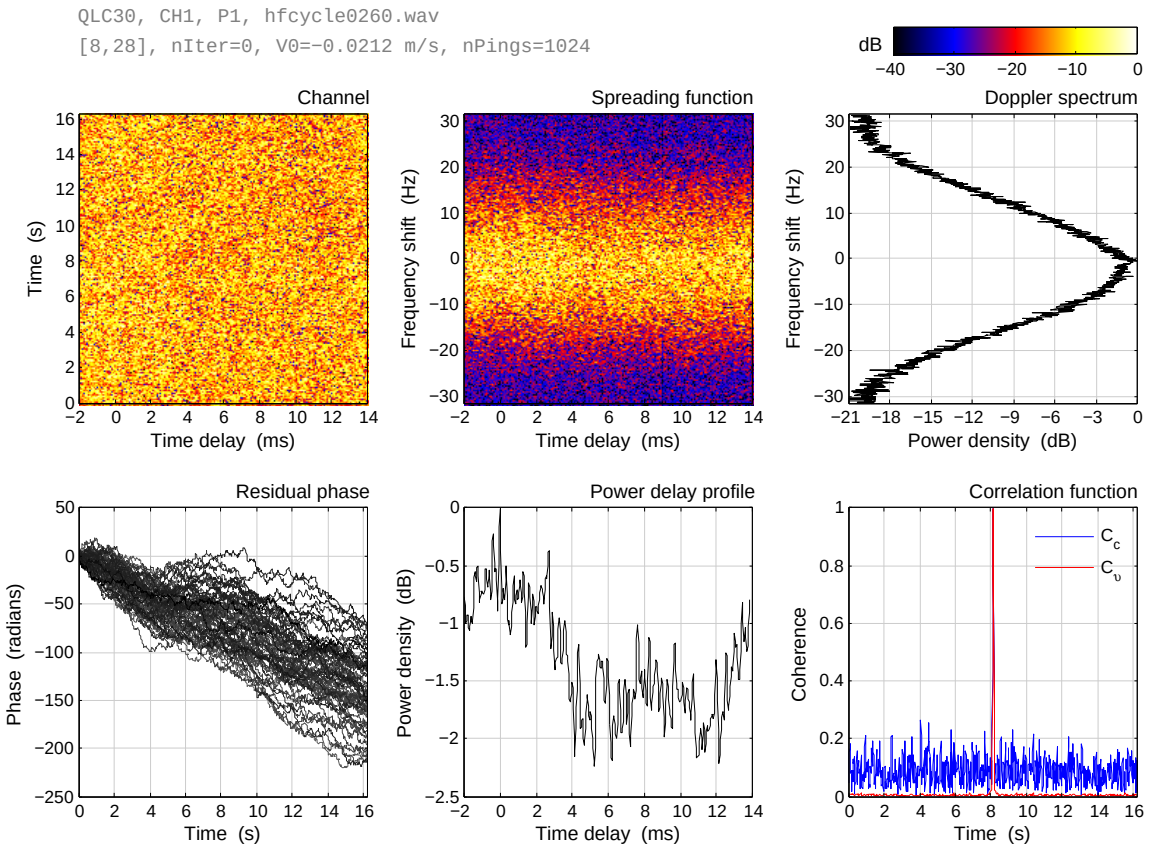

Figure 5.4 Channel D. Overspread channel.

5.5 Channel E

Like channel B, channel E features a stable path that dominates the Doppler spectrum. The interesting part concerns the delayed arrival at $\tau = 12$ ms, which ceases to exist at $t = 24$ s. The diffuse scattering elsewhere in delay diminishes, and soon after the path at $\tau = 4$ ms also weakens. A non-stationary channel results, over the 32-s observation window.

The attenuation coincides with the sudden onset of a wind burst, with the wind speed increasing from 5 m/s to 15 m/s. The striking part is that the attenuation sets in almost instantaneously, within a few seconds. Significant waves do not build up this fast, as confirmed by waverider measurements (Sec. 6.3). However, the waverider has a cut-off frequency at 0.6 Hz and does not register high-frequency ripples on the sea surface. Ripples may form quickly and are a candidate mechanism to account for the increased surface losses. Another candidate is the formation of a bubble screen. A squall of similar strength was shown to populate the top few meters of Loch Ness with air bubbles within a time span of 2 minutes (Fig. 6a in [19]).

The wind burst causes a drop in signal level and an increase in noise level, lowering the SNR by 10 dB. Nonetheless the channel becomes a more benign communication channel during the burst, see Sec. 6.3.

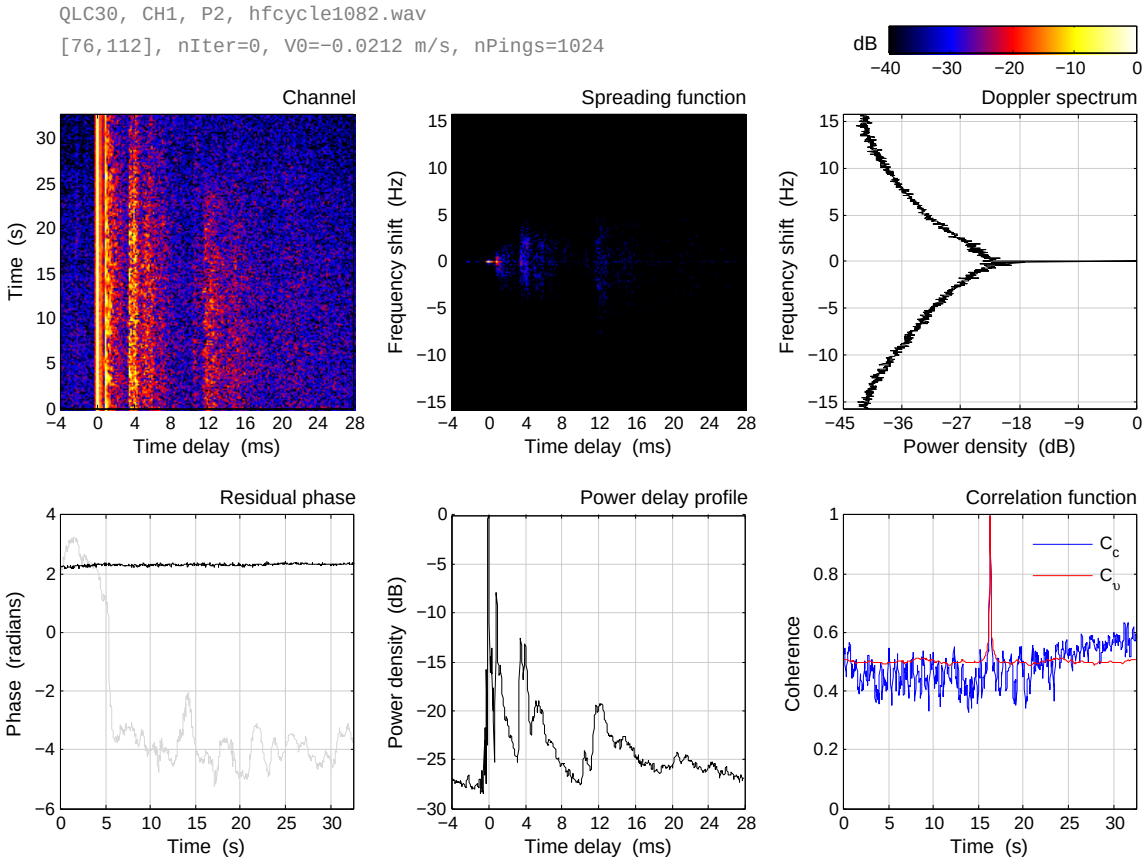

Figure 5.5 Channel E. The spreading function is shown on a different scale in Fig. A.5.

5.6 Channel F

Channel F concerns the same deployment as channel E, but was sounded three days later. It is a remarkable channel. Figure 5.6 zooms in on the first few paths and reveals an arrival with a time-varying time delay. This path shifts from zero delay to $\tau = 2$ ms in a cyclic fashion. The repetition time of 3 s agrees with the period of the dominant waves at the time of this sounding, while the sweep duration of ≈ 8 s is of unknown origin.

A time-varying time delay with stationary instruments has previously been reported by Preisig and Dean for experiments in the surf zone [18]. In their case the paths move back and forth, whereas the path in the present channel does not return. It just stops at a 2-ms delay. This results in a net frequency shift as observed in the spreading function. Indeed, the increasing delay is equivalent to an increasing acoustic path length, which gives rise to the familiar Doppler effect. The contribution of the wandering path to the total Doppler spectrum shifts its center of gravity to below 0 Hz and leads to asymmetry. As an excursion of 2 ms corresponds to an acoustic path length difference of 3 m, whereas the significant wave height was 1 m during the sounding, it is difficult to account for the phenomenon solely by up-down motion of the waves. The wave direction was approximately perpendicular to the acoustic track, and left-right motion in the horizontal plane may be involved [18]. Air bubbles due to breaking waves may also play a role.

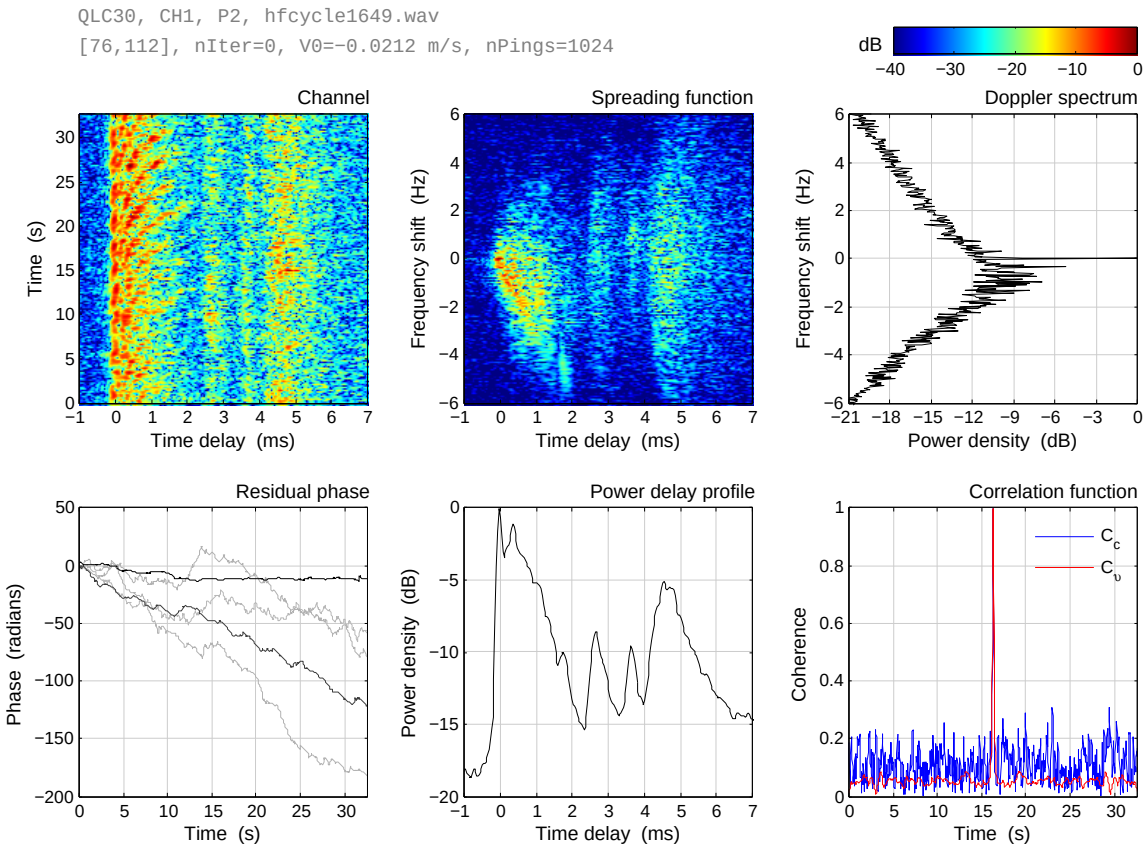

Figure 5.6 Channel F. A time-varying time delay with a Doppler shift.

5.7 Channel G

A more extreme case of frequency shifting is provided by the sounding of channel G, which is the same channel that was used for Fig. 4.4. A frequency offset is manifest irrespective of time delay, and the accumulated Doppler spectrum is asymmetrical with a center of gravity at $\upsilon = +1.5$ Hz. Like channel F, channel G features a specular peak at $\upsilon = 0$. Such peaks confirm proper calibration of the frequency axis, ensuring that apparent shifts are not due to clock frequency offsets. Unlike channel F, channel G does not provide visual clues in the $h(\tau, t)$ panel as to the origin of the shifting.

The specular path has a constant phase in the bottom-left panel of Fig. 5.7. All other phase measurements have a positive gradient. There is no time compression in this stationary channel, and a receiver does not receive more bits per unit of time than transmitted by the transmitter. There is only a continuous phase drift. Adaptive equalizers benefit from a phase-locked loop: Sec. 6.4.

There is no obvious relation between wind/wave direction and the sign of the frequency shift. In the case of channel G, the positive shift occurs for transmission downwind, but other soundings (not shown) have yielded a negative shift for downwind transmission. Likewise, upwind transmissions have yielded both positive and negative shifts. Fig. A.6 illustrates the complexity of the phenomenon with a spreading function that simultaneously features negative and positive shifts.

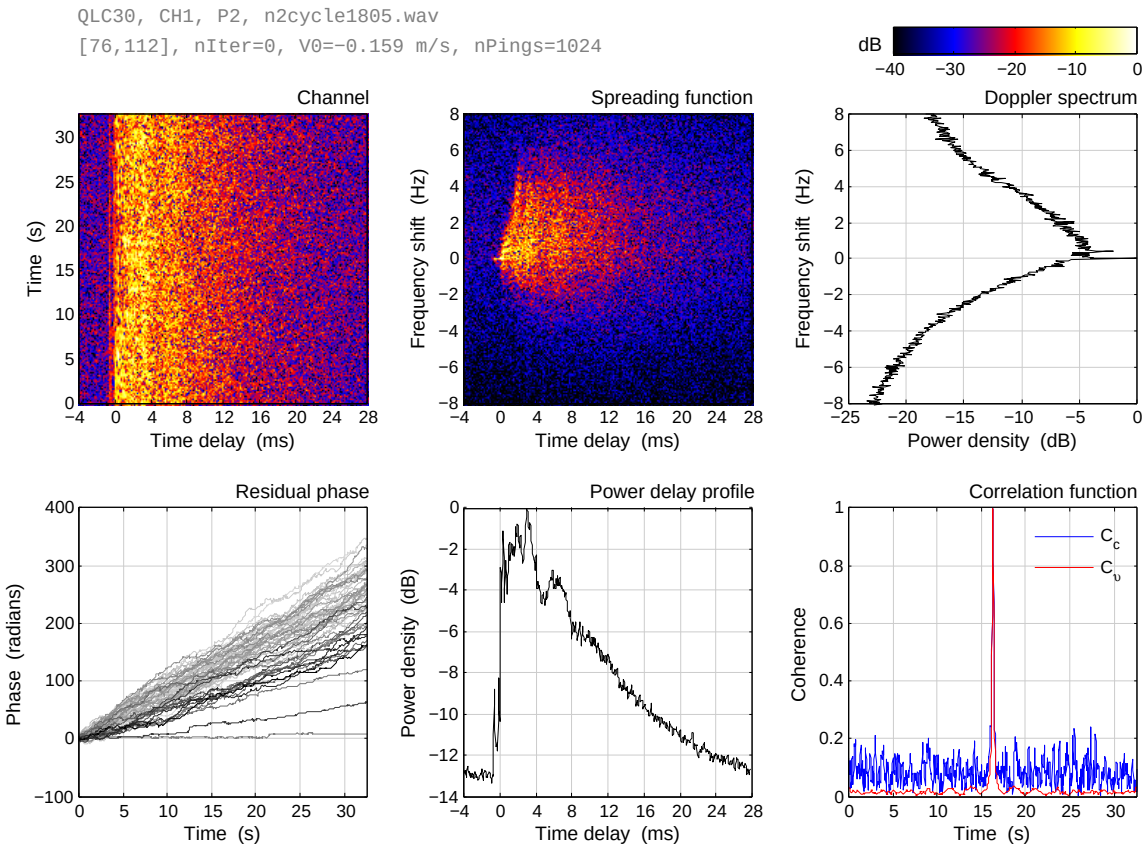

Figure 5.7 Channel G. Distortion and offset of the Doppler spectrum.

5.8 Channel H

Previous comparisons for a fixed geometry (B–C, E–F) revealed significant variation in scattering statistics over time. H concerns the same deployment as G and again illustrates the variability of the medium. There are two days between the G and H soundings, with the main difference being wind and wave conditions. H is a completely different channel from G. There are three main arrivals, two of which experience deep fading. The strongest arrival has no deep fades, but its phase varies more than in many other channels, for instance, A, B, C, and E. The Doppler spectrum has become sharply peaked, symmetrical, and without noticeable offset.

The fading of the arrivals at $\tau = 1$ and 3 ms resembles a switch off/on effect; whenever the paths return they have the same phase as before. This causes a periodic structure in the correlation functions, in a similar fashion to channel C. However, where C was sounded in the presence of ship-induced waves, the periodicity for H is related to wind-generated waves. Waves due to wind have a wider spectrum and consequently the fading pattern is less regular. Once again a coherence time $\mathcal{C}_{0.5}$ is ill-defined, with C_c dropping below 0.2 and rising to above 0.6 again. C_v has an oscillatory component but is not quite the same as C_c. There is correlation between the fading arrivals in this non-WSSUS channel, whose full power delay profile is shown in Fig. A.7.

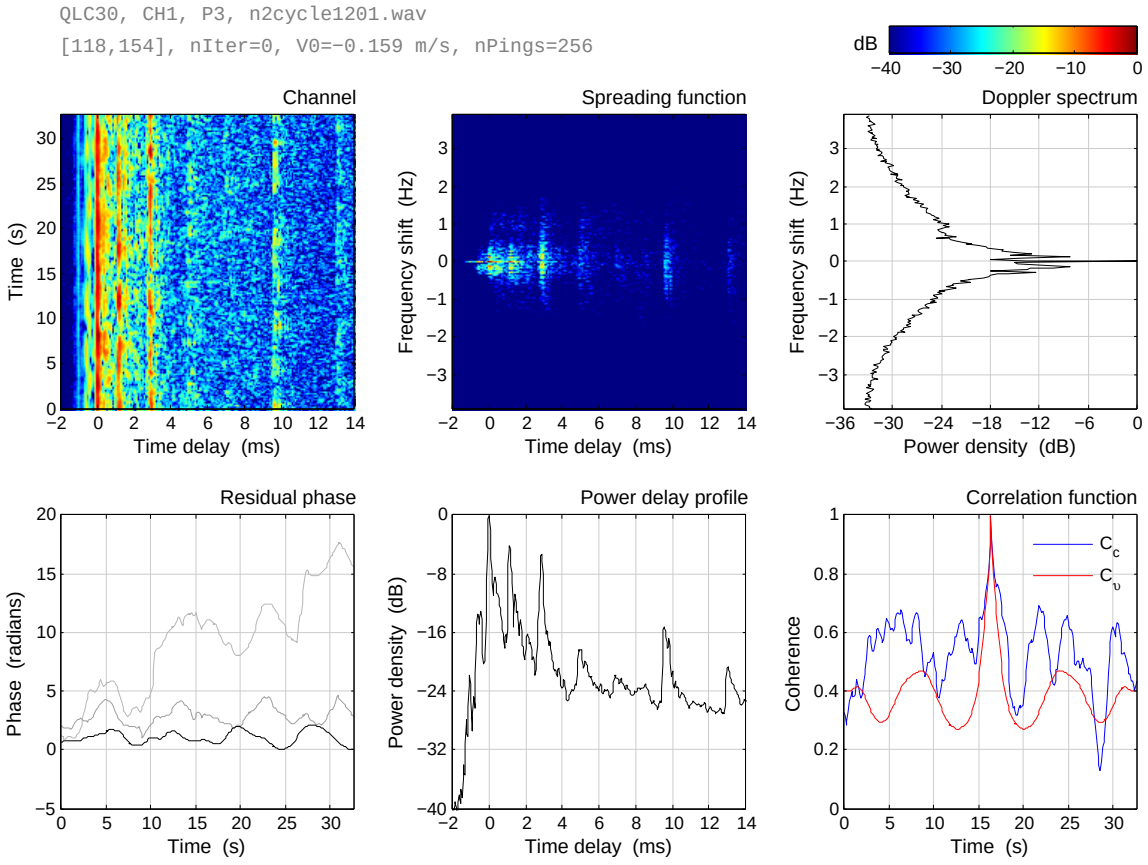

Figure 5.8 Channel H. Correlated scattering and cyclostationary paths.

5.9 Channel I

Until this point all geometries were static, and frequency spreading and shifts had to be accounted for by changes of the propagation medium itself. Channel I differs in that it represents a channel between surface ships. The transmitter was towed by a sailing ship, and the receiver deployed from an anchored ship. This is the same channel that was examined and mimicked in [4].

The power delay profile is a dense crescendo of multipath arrivals with the most energetic paths toward the end, which is characteristic of propagation in the sound channel that characterizes the Baltic Sea in late summer. Figure 5.9 results from placing the center of gravity of the Doppler spectrum at $\upsilon = 0$ Hz, as explained in Sec. 4.4. This requires $V_0 = 2.52$ ms. However, removal of a constant speed does not eliminate time-varying Doppler shifts (TVD). This is evident from the phase measurements, which reveal an undulating phase component that is the same for all paths. It reflects motion of the transmitter ship on the waves, which is transferred onto the towed source. There is a considerable mismatch between C_c and C_υ, and the reason is that the Doppler spectrum is dominated by TX/RX motion. Channel I is non-WSSUS because i) there is phase correlation between arrivals, and ii) wandering of paths in delay renders it non-stationary. The latter is difficult to tell from Fig. 5.9, but will be more clear for channel J.

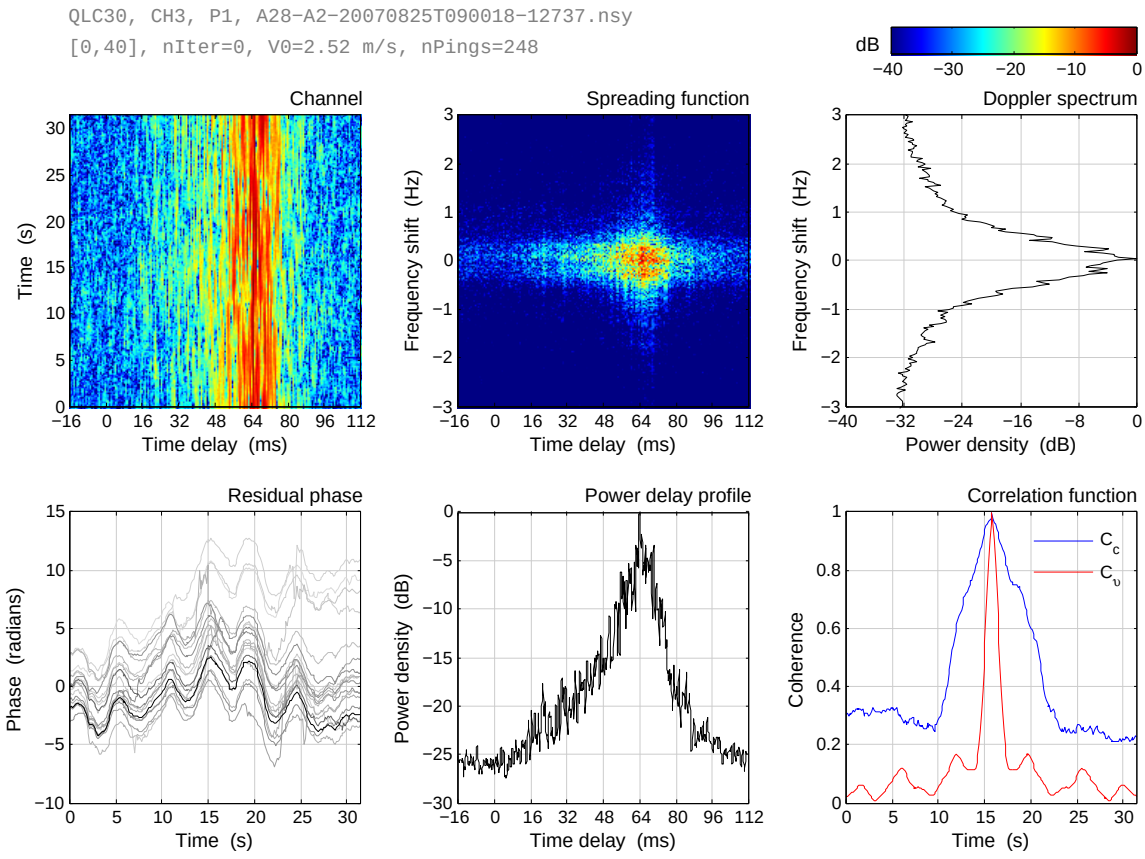

Figure 5.9 Channel I. Transmission in a sound channel with a towed source.

5.10 Channel I.2

The TVD of channel I can be removed by the iterative procedure described in Sec. 4.4. To this end, the phase measurement of the strongest arrival in Fig. 5.9 is used to resample the data with a time-varying resampling factor. Fig. 5.10 indeed shows that the phase of this path has become constant, and also that the phase correlation among arrivals has disappeared. The result is a significant narrowing of the spreading function and Doppler spectrum. Doppler spread values are smaller for all definitions, see Table 5.2.

Moreover, C_υ has approached C_c and yields a good match and the same coherence time. Before TVD removal C_c is shaped by fading processes, whereas C_υ is dominated by Doppler variance due to TX/RX motion. After TVD correction, both correlation functions are governed by fading, because fading is the only mechanism left to yield Doppler spreading. The narrowing of the Doppler spectrum broadens its inverse Fourier transform, C_υ. TVD compensation has changed the channel from non-stationary to stationary, over the 30-s window. On a longer time scale the channel would be non-stationary, as the impulse response is generally a function of range and depth. In this case the tow ship sails away from the receiver, so the range increases. A property of propagation in the sound channel is that individual paths have the same fading rate, essentially the same Doppler spectrum before TVD removal, and essentially the same Doppler spectrum after TVD removal.

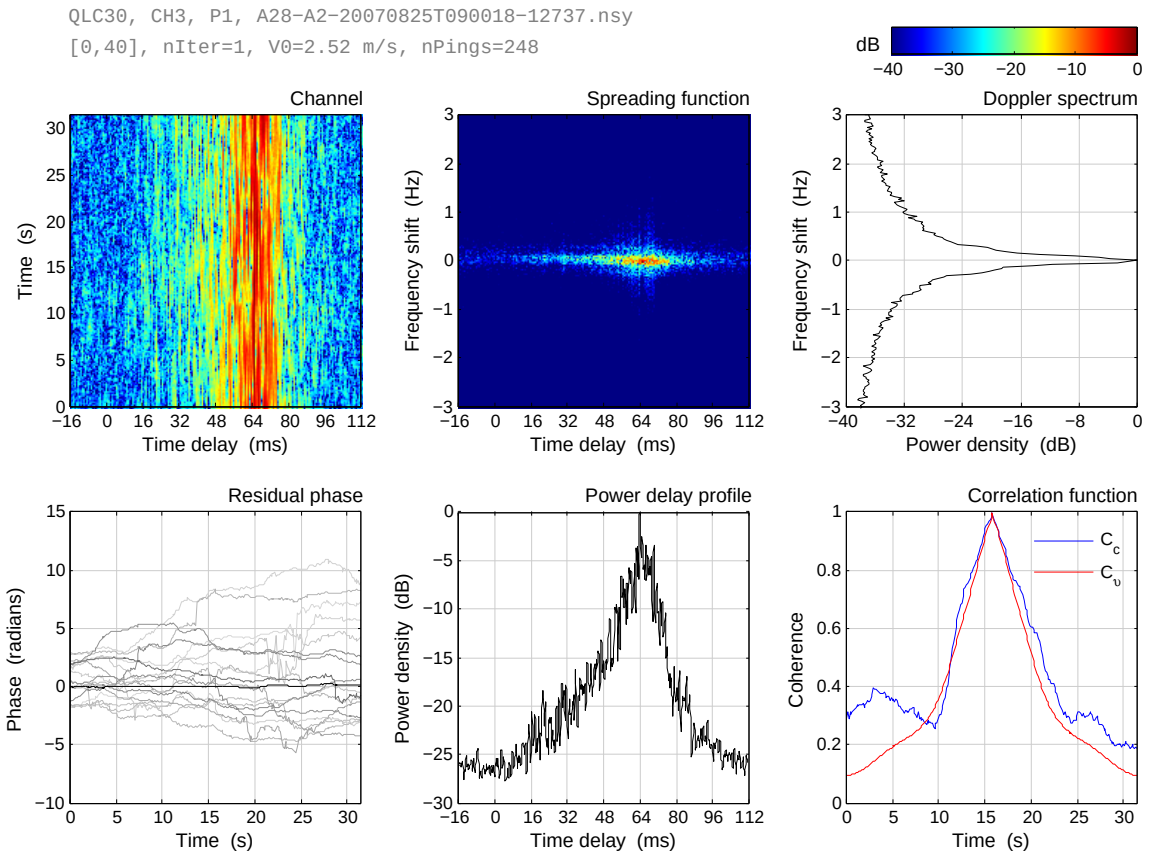

Figure 5.10 Channel I, after elimination of the time-varying Doppler shift.

5.11 Channel J

Soon after the sounding of I, a similar experiment was conducted on the Norwegian continental shelf. A smaller tow ship and higher waves result in a strongly undulating phase. Channel J is shown because it clearly illustrates the time compression/dilation that is inextricably bound up with wideband signaling in the presence of TX/RX motion. Multipath arrivals wander back and forth in delay. $C_c(\Delta t)$ goes up and down, but for a different reason than in channels C and H. In those channels the periodic rising is due to fading and reappearing arrivals at a fixed delay. In channel J, it is due to paths with a constant (or slowly varying) amplitude that wander in delay. Note in this regard that $C_c(\Delta t)$ is the *zero-lag* cross-correlation. The Doppler spectrum is totally dominated by TX/RX motion. It is wide, with a rapid falloff that is steeper than the flanks of a Gaussian, and $C_v(t)$ is correspondingly narrow.

The effect of TVD removal is shown in Fig. A.8. For this channel the resampling procedure requires two iterations, but it manages to completely level the phase of the chief arrival. The phase of the other paths is also flattened, although there is one arrival, the upper curve in the graph, that still bears evidence of the ship motion. The wandering paths are straightened, the troughs in C_c have disappeared, and a dramatic narrowing of the spectrum yields a C_v that, although not identical to C_c, is now in the same ballpark.

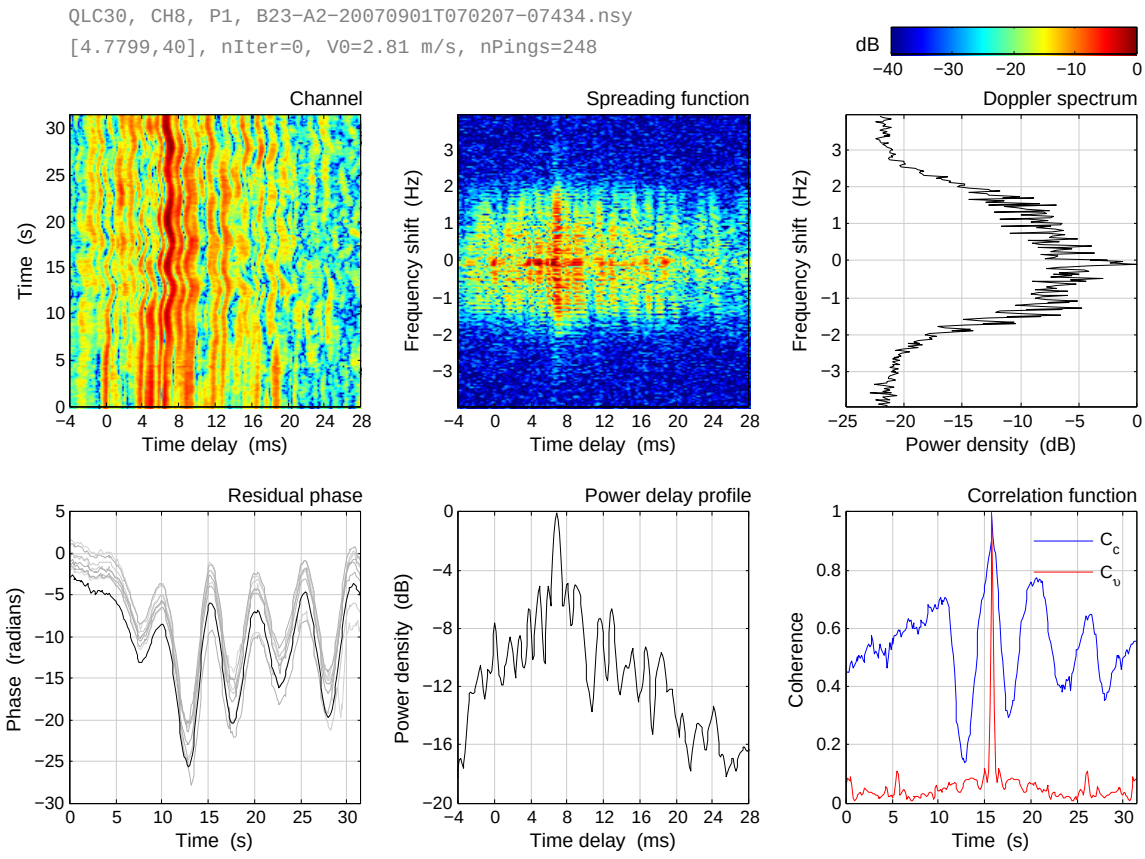

Figure 5.11 Channel J, after correction for a constant velocity V_0.

5.12 Channel K

TX/RX motion introduced a time-varying range rate that was virtually the same for all propagation paths in channels I and J. Channel K features markedly different residual (i.e., after removal of the nominal velocity V_0 by resampling) range rates for a sounding in the Bjørnafjord at a relatively large depth/range ratio. The spreading function in Fig. 5.12 features a series of dots in delay-Doppler space. The main paths are sparse in delay, have different frequency shifts, and their phases would drift away from one another if properly measured. In this case the phase measurement is not proper, since the main paths in the $|h(q,n)|^2$ panel are slowly diverging and converging: see Fig. A.9. Their phase is strictly measured along fixed tap positions, which makes no sense when paths walk away. Despite the non-WSSUS character, the two correlation functions are the same.

$\mathcal{T}_{\text{thr, }-10\text{ dB}}$ exceeds 100 ms, but $\mathcal{T}_{\text{rms}}$ and $\mathcal{T}_{\text{en, }90\%}$ cannot be measured because the sounding is severely aliased. The received signal has a long reverberation tail, lasting seconds, that corrupts the measured power delay profile. Although the main paths are sparsely distributed, in delay and in Doppler, the overall channel is not sparse. The cyclicity of the power delay profile makes it difficult to guess the order of arrivals in this kind of channel. In such cases $h(q,0)$ and $h(q,N-1)$ may be inspected separately, or different kinds of probe signals may be consulted, such as a single chirp transmitted just before or after the sounding probe. Fig. 5.12 shows the arrivals in the correct order.

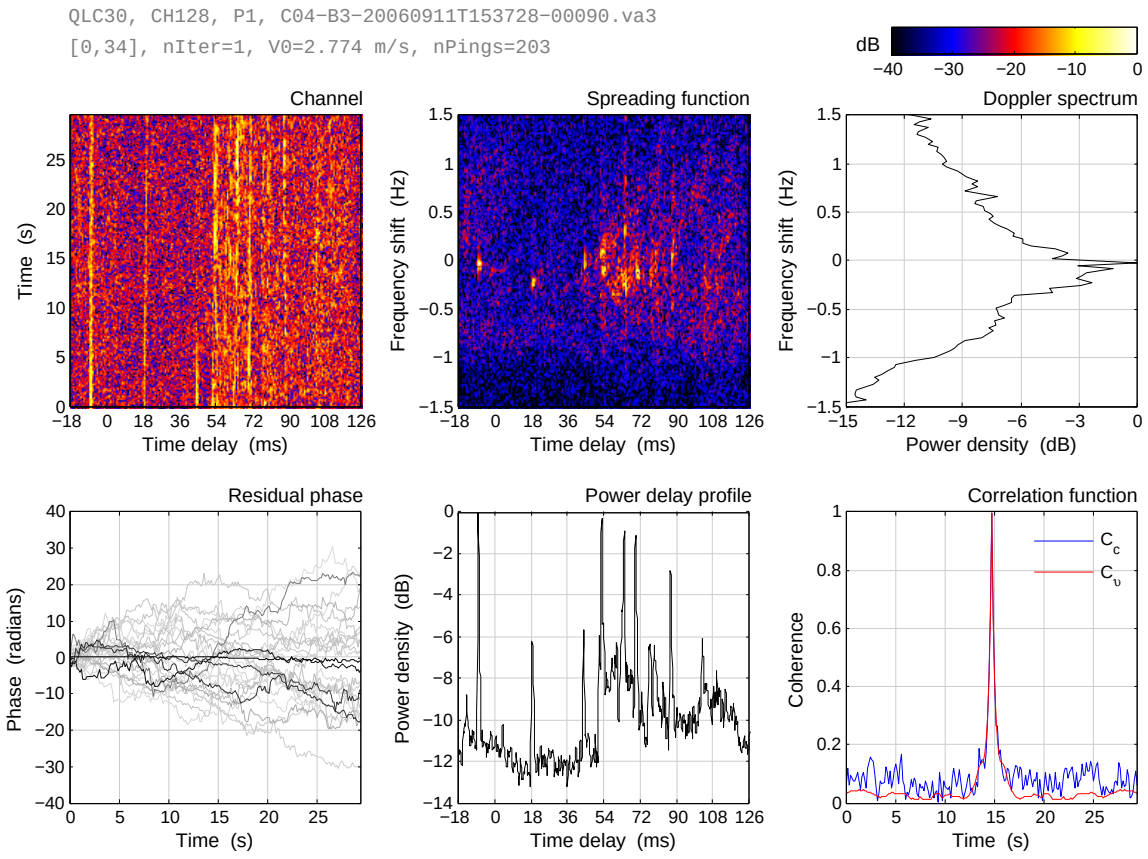

Figure 5.12 Channel K, featuring range-rate variation between paths.

5.13 Channel L

Channel L originates from a sea trial near Kauai in the Pacific Ocean [31]. Transmission was between a source towed by a surface ship, and one of the elements of an anchored vertical hydrophone array. Resampling using the phase of the strongest path does not work for this channel, because the path has deep fades that lead to discontinuities in the phase measurement. Instead, the resampling (Eq. 4.10) is applied with a phase averaged over several paths. However, the TX/RX motion is not the main property of interest of channel L. This channel features a number of arrivals, or clusters of arrivals, with i) a power density that decreases with delay; ii) a smearing in delay that increases with delay, iii) a Doppler spread that increases with delay. Similar effects can be noticed in some of the previous channels, but not as clearly as in this Kauai channel.

Successive arrivals have experienced more surface interactions, and/or have been scattered at larger grazing angles, which accounts for the increase in Doppler spread with delay. Similarly, the decreasing amplitude is due to path losses that generally increase with travel distance and the number of boundary interactions. As in some of the previous channels, the Doppler spectrum is sharply peaked and heavy tailed, and is somewhat asymmetrical. There is a fairly good match between the two correlation functions.

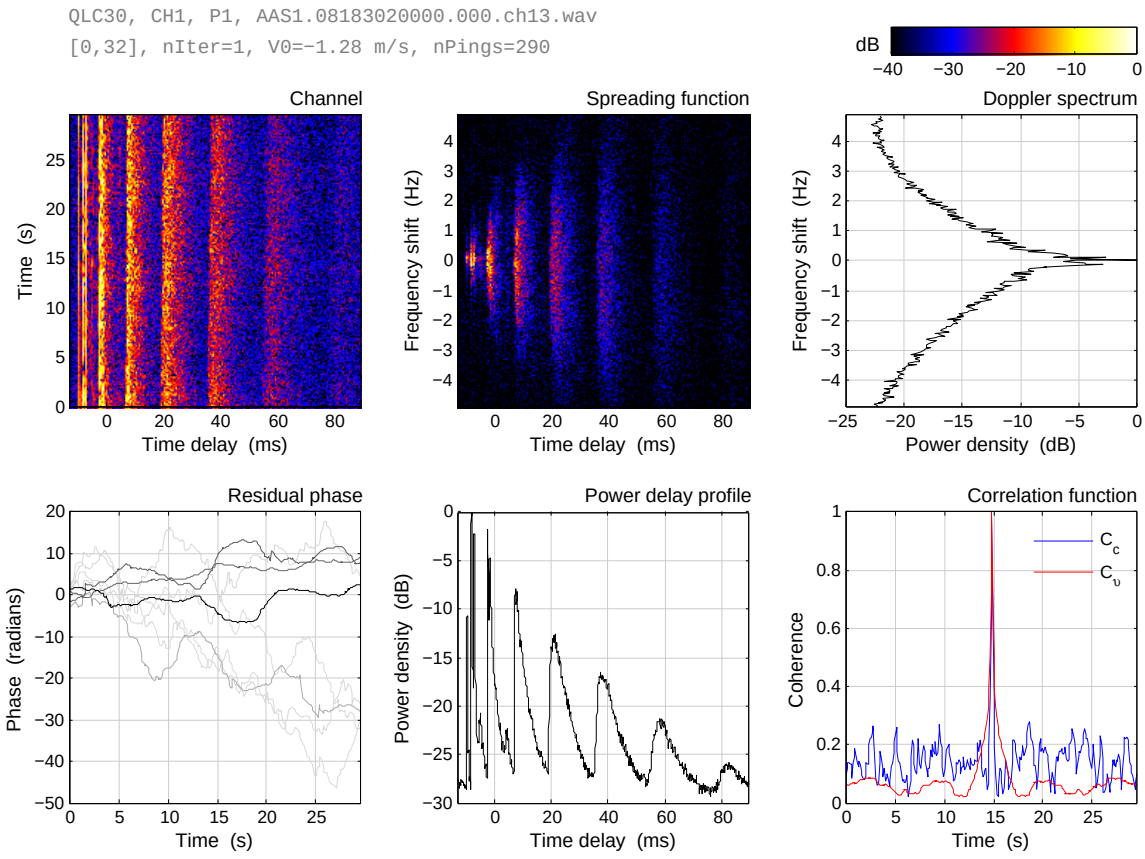

Figure 5.13 Channel L. Data courtesy of H. C. Song of Scripps Institution of Oceanography.

5.14 Channel M

The last sounding is from an experiment on the Norwegian continental shelf. Transmission was between a source and receiver towed by platforms sailing approximately parallel tracks at the same speed. Hence the nominal Doppler shift $V_0 = 0.036$ m/s is small. The channel is shown after removal of the constant shift; the frequency spread of the first two arrivals evidences some residual TVD. However, the Doppler spectrum (a compressed exponential, see Sec. 7.1) is dominated by the bulk of trailing arrivals, which have interacted with the sea surface. Channel M is a fine example of a sounding where T is ideally balanced to capture most of the spread in delay and in frequency. Later soundings from the same experiment, after the wind picked up, reveal overspread channels.

Like several of the previous channels, M can hardly be called sparse in delay. Sparsity is normally understood to mean that a large fraction of the total signal power is furnished by a limited number of discrete arrivals, a condition exploited by some channel estimation algorithms. For a specific communication system to deliver, a sufficient fraction of the energy is to be furnished by sufficiently few arrivals, or sufficiently few/small delay intervals. This depends on the data rate. A low-rate system can tolerate a high degree of self-interference and can operate on a small fraction of the total signal energy. High-rate systems need to harvest most of the signal energy, in delay and in Doppler, and for this category sparsity seems less common than often assumed.

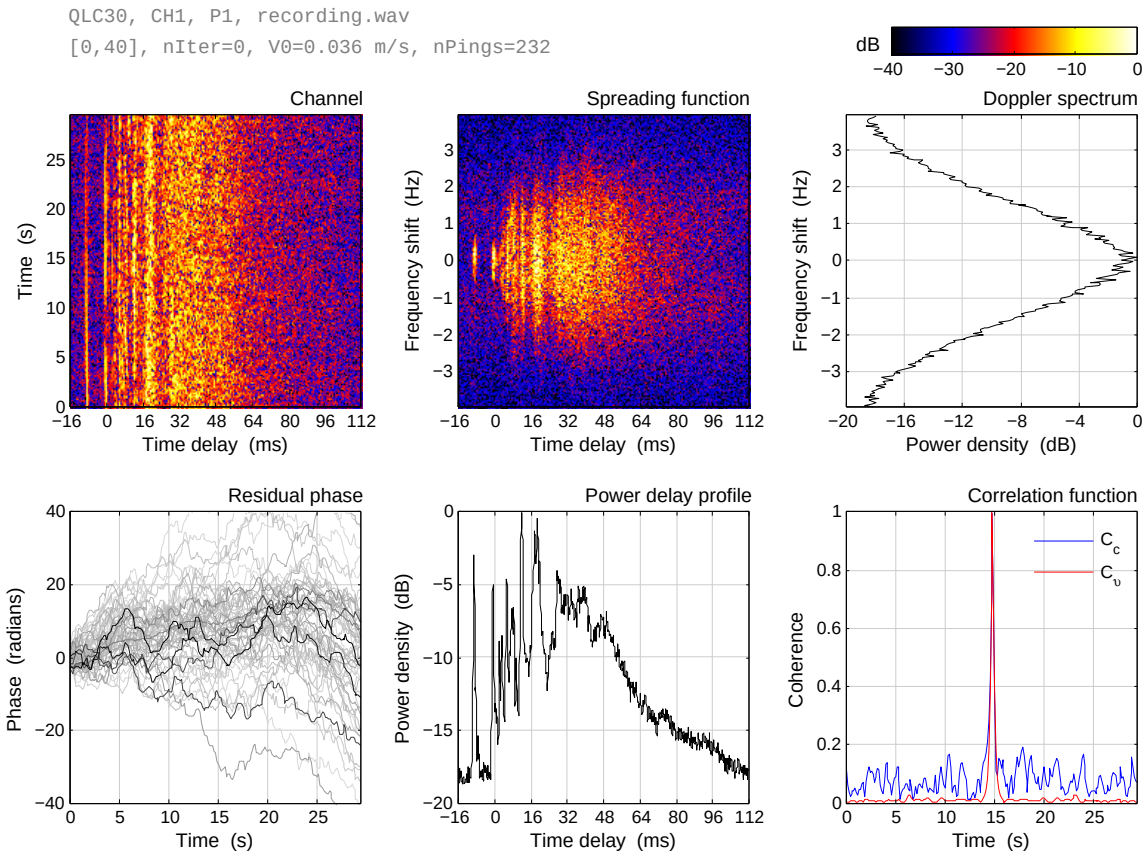

Figure 5.14 Channel M. Figure courtesy of H. S. Dol of TNO.

5.15 Summary

Table 5.2 summarizes the channels in terms of delay spread, Doppler spread, and coherence time. There are sizable differences between channels and for a given channel between definitions. The table makes clear that these parameters should be defined upon use. Threshold definitions tend to be insensitive to the long reverberation tail that may characterize the power delay profile, e.g. channels D, E, F, H, K, and whose importance for communication systems increases with the data rate. Channel snapshots obtained from a single chirp and plotted on a linear scale can be misleading, as such tails can go unnoticed. Averaging over time is essential for the power delay profile, and a logarithmic scale is preferred for presentation. The use of a threshold definition for the Doppler spread may be a bad idea in the presence of a dominant specular peak.

The table also illustrates that the coherence time $\mathcal{C}_{0.5}$ often cannot be measured. In some cases because the correlation function does not drop below 0.5 during the limited sounding time, in other cases because it crosses the threshold value multiple times. A criterion $\mathcal{C}_{0.8}$ [9] can be used instead for the former category but is no structural solution. There are also channels where the specular energy is 80 or 90 percent of the total. A single coherence time can only characterize a channel when the correlation function has a known shape, e.g. a Gaussian for a Gaussian Doppler spectrum. In the presence of a specular base level, a spread-spectrum communication system may operate satisfactorily without channel tracking even when $\mathcal{C}_{0.5}$ is short, whereas a high-rate system may require fast tracking even when $\mathcal{C}_{0.5}$ is infinite. See Sec. 6.2 for an illustration.

Ch.	$\mathcal{T}_{\text{thr, –10 dB}}$	$\mathcal{T}_{\text{rms}}$	$\mathcal{T}_{\text{en, 90\%}}$	$\mathcal{D}_{\text{thr, –10 dB}}$	$\mathcal{D}_{\text{rms}}$	$\mathcal{D}_{\text{en, 90\%}}$	$\mathcal{C}_{\text{c, 0.5}}$	$\mathcal{C}_{v\text{, 0.5}}$
A	0.3 ms	2.9 ms	0.3 ms	0.0 Hz	0.1 Hz	0.0 Hz	—	—
B	4.0 ms	6.3 ms	17 ms	0.0 Hz	1.4 Hz	3.2 Hz	—	—
C	6.4 ms	5.7 ms	13 ms	0.0 Hz	0.8 Hz	1.5 Hz	—	—
D	79 ms	50 ms	129 ms	30 Hz	8.0 Hz	26 Hz	29 ms	27 ms
E	1.0 ms	7.0 ms	18 ms	0.0 Hz	2.7 Hz	8.2 Hz	—	—
F	5.5 ms	7.4 ms	21 ms	2.1 Hz	3.8 Hz	13 Hz	69 ms	73 ms
G	18 ms	6.8 ms	21 ms	4.6 Hz	3.7 Hz	11 Hz	102 ms	96 ms
H	3.1 ms	12 ms	13 ms	0.24 Hz	0.68 Hz	1.8 Hz	—	—
I	21 ms	13 ms	35 ms	0.70 Hz	0.41 Hz	0.79 Hz	4.8 s	0.84 s
I.2	21 ms	13 ms	34 ms	0.13 Hz	0.32 Hz	0.19 Hz	5.0 s	4.4 s
J	19 ms	24 ms	64 ms	3.2 Hz	1.0 Hz	3.2 Hz	—	0.20 s
J.2	17 ms	22 ms	53 ms	0.06 Hz	0.68 Hz	1.1 Hz	—	11 s
K	134 ms	—	—	2.0 Hz	1.1 Hz	4.0 Hz	0.23 s	0.22 s
L	16 ms	21 ms	50 ms	1.1 Hz	1.4 Hz	4.9 Hz	0.15 s	0.21 s
M	64 ms	24 ms	76 ms	3.5 Hz	1.0 Hz	3.4 Hz	0.22 s	0.22 s

Table 5.2 Delay spread, Doppler spread, and coherence time. A dash is used when measurement is impossible or ill-defined.

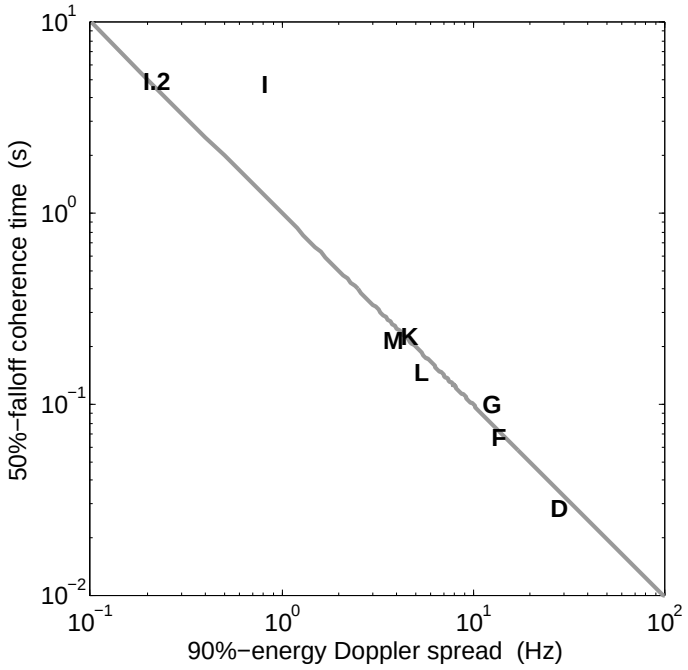

Figure 5.15 Coherence time $\mathcal{C}_{c,\,0.5}$ versus $\mathcal{D}_{en,\,90\%}$.

The channel coherence time is often taken to be the inverse of the Doppler spread, but which coherence time is the inverse of which Doppler spread is a matter of definitions. When the coherence time $\mathcal{C}_{\mathrm{c},0.5}$ is measurable, it is approximately the inverse of the 90%-energy Doppler spread: Figure 5.15. The single outlier is channel I before removal of kinematic effects. This illustrates that one should be careful with linking coherence time and Doppler spread in the presence of transceiver motion. Obviously this outlier would be no outlier if $\mathcal{C}_{\upsilon,0.5}$ were used, but $\mathcal{C}_{\mathrm{c},0.5}$ may be a more accurate estimate of the true coherence in such channels.

Table 5.3 presents a statistical characterization of the channels in terms of stationarity, correlation, and separability of the spreading function. These properties are not determined according to rigorous criteria, but to a first approximation and as far as one can tell from the data. The message is not that each channel strictly falls in a category, but that there exists a huge variation in statistical properties of acoustic channels.

Stationarity is judged from inspection of subperiods of the channel (e.g., does the second half of the sounding yield similar results as the first half), and from the correspondence between C_υ and C_c. In all cases the stationarity is judged over the sounding duration. On a long enough time scale all shallow-water channels are non-stationary. The channels labeled cyclostationary are not cyclic in the sense that the correlation function repeatedly reaches unity (channel C is close though), but they have cyclostationary features that are important for the overall characterization.

Correlation is examined by computation of correlation coefficients for the complex channel taps. For instance, Fig. A.3 compares channels B and C, where B is said to have uncorrelated scattering and C correlated scattering. Correlation does not need to be zero-lag in order to count as correlated

Ch.	Scattering		Separable
A	stationary	—	yes
B	stationary	uncorrelated	no
C	cyclo+non-stationary	correlated	no
D	stationary	uncorrelated	yes
E	non-stationary	uncorrelated	no
F	(cyclo)stationary	uncorrelated	no
G	stationary	uncorrelated	no
H	cyclo+non-stationary	correlated	no
I	non-stationary	correlated	yes
I.2	stationary	correlated	yes
J	non-stationary	correlated	yes
J.2	non-stationary	correlated	no
K	non-stationary	uncorrelated	no
L	stationary	uncorrelated	no
M	non-stationary	uncorrelated	no

Table 5.3 Stationarity, correlation between paths, and separability.

scattering. Channels I and J are in a gray area after TVD removal. Phase correlation is removed, but there is still amplitude correlation between some paths. Since there are many paths and since the sounding duration is not long compared to the time scale of fading, the measured correlation could be coincidental. There are always paths that move in tandem when the observation time is short.

6 Implications for communications

For some channels (A, B, D, E, and G), the sounding results are used to aid understanding of the performance of a communication system. This section considers a direct-sequence spread spectrum (DSSS) waveform that was transmitted in tandem with the channel probe signals. Parameters include a 7-chip spreading code, a chip rate of 3500 cps, a 14-kHz carrier, and a raw data rate of 1000 bps. The single-hydrophone receiver is a chip-rate decision-feedback equalizer. It is operated in training mode, spans 12 ms, and employs the recursive-least-squares tap update algorithm. Output QPSK constellations and SINRs are shown after equalizer convergence and after despreading. The receiver input SNR is about 3 dB below the SNR mentioned for the probe signals in Table 5.1.

6.1 Benign versus overspread channel

The easiest channel among the 14-kHz soundings is A and the most difficult one is D. Figure 6.1 shows the symbol constellations at the receiver output. The output SINRs are +38 and –2 dB, respectively, yielding an immense 40-dB performance difference. D also has a lower input SNR, but there is good reason to believe that performance would not improve much if D had access to

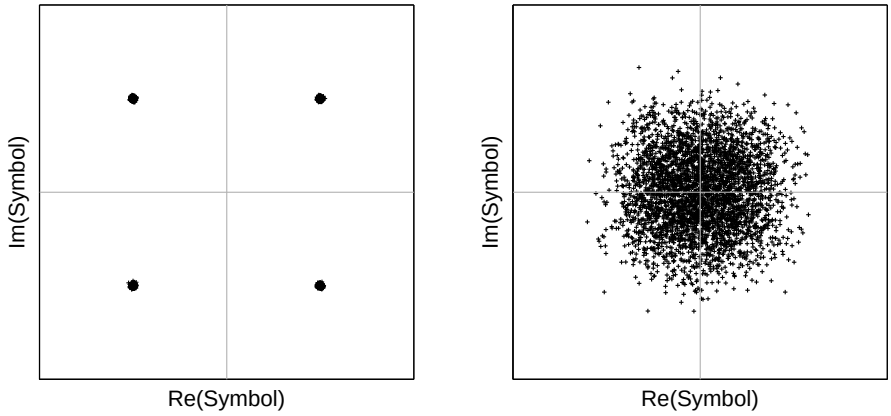

Figure 6.1 Receiver output constellation in channel A (left) and channel D (right).

the SNR of A. Conversely, if A is combined with the SNR of D the system becomes noise limited. Bandwidth use is inefficient in channel A, as this channel supports much higher data rates. By contrast, the constellation of channel D implies that the data rate has to be lowered significantly to achieve an acceptable BER.

6.2 Performance prediction

The shape of the correlation function of channel B allows a simple performance prediction for an equalizer deprived of channel tracking. The symbol constellation is plotted in Fig. 6.2. If tap updates are stalled after initial training, the receiver maintains an output SINR of 9.6 dB. Channel tracking is not required, as the stable, specular paths carry sufficient power. The output SINR rises to 13.8 dB with continuous channel tracking, which demonstrates that the adaptive equalizer can harvest part of the Doppler-spread signal power within its span. A rough performance prediction for the first scenario is possible by observing that i) the specular energy is 60% of the total in channel B; ii) the communication scheme has a spread-spectrum gain of 7; iii) the input SNR is very high such that the system is limited by self-interference. On the assumption that the receiver can coherently

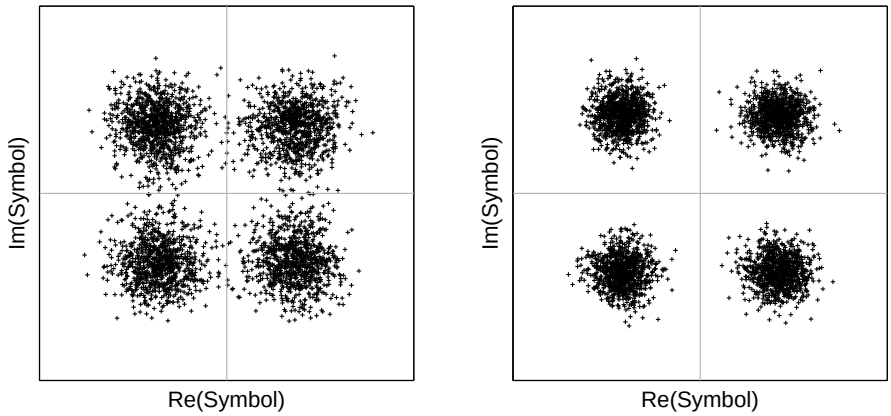

Figure 6.2 Constellations without (left) and with (right) continuous channel tracking.

combine all the energy of the static paths and none of the fading arrivals, the Doppler-spread energy acts as interference. Under these assumptions the output SINR becomes $10\log_{10}(0.60/0.40) + 10\log_{10}(7) = 10.2$ dB, close to the measured SINR. The accuracy may be coincidental, but not the fact that tracking is not required at 1000 bps in channel B. An initial channel estimate suffices. The 4-dB increase in output SINR illustrates that continuous tracking supports a higher data rate.

6.3 Effect of a wind burst on a communication channel

Implications of the squall that caused the non-stationarity of channel E are investigated in Fig. 6.3. The figure shows the wind measurement, significant wave height (in the 0.06–0.6 Hz band), the in-band sound pressure level (SPL), the 90%-energy delay spread, 90%-energy Doppler spread, and receiver output SINR, all plotted versus time of day. The wave height is obtained from the heave measurement of a waverider buoy deployed close to the acoustic receiver. It responds to the wind, but slowly as it takes time for waves to build up. SPL is plotted for signal and noise separately. The delay spread is measured with a 128-ms LFM probe and the Doppler spread with a 16-ms PRBS. Each signal was transmitted once every six minutes. The wind sensor is about 1 km from the acoustic track, which may cause a timing offset between the wind measurement on the one hand, and the waverider and acoustic measurements on the other. At any rate, the wind burst rapidly lowers the signal level and slowly increases the noise level, *reducing* the receiver input SNR by ≈ 10 dB. Simultaneously the receiver output SINR *rises* by ≈ 10 dB. The cause is a dramatic reduction in the channel delay spread and Doppler spread, due to the attenuation of delayed, surface-interacting arrivals. Clearly the communication system is not limited by noise, but by the channel.

The wave height (in the 0.06–0.6 Hz band) and the noise level respond slowly to the wind, whereas signal level, delay spread, Doppler spread, and output SINR respond quickly. These quantities start to return to "normal" before the end of the squall, which might suggest a transient switch-on effect. Although their response is fast, Fig. 6.3 makes clear that the time for quantities to reach their minimum/maximum values is actually longer than the few seconds suggested by the sounding of Fig. 5.5, which was recorded at 21:39. Whether it is high-frequency surface ripples and/or a screen of air bubbles that cause the acoustic effects, it is clear that wind does not necessarily render an acoustic communication channel more difficult.

Figure 6.4 exhibits the delay profile and Doppler spectrum before and during the wind burst. The data are not separately normalized, such that the relative power densities are compared. The specular path is not affected by the wind but has even become slightly stronger (the source level of the transmitter was constant). Everywhere else in delay and Doppler the power density has decreased by 10–15 dB. Since the cause of the reverberation is surface scattering, attenuation of the scattered energy simultaneously reduces the delay spread and the Doppler spread. The enhanced output SINR is welcome, more realistically it rather points to the inability of the receiver to effectively harvest the available signal energy before and after the wind burst. A large part of the signal power acts as interference. Concerning channel simulation for communications, it would be more important to be able to model Doppler-spread reverberation tails than the (onset of a) wind burst.

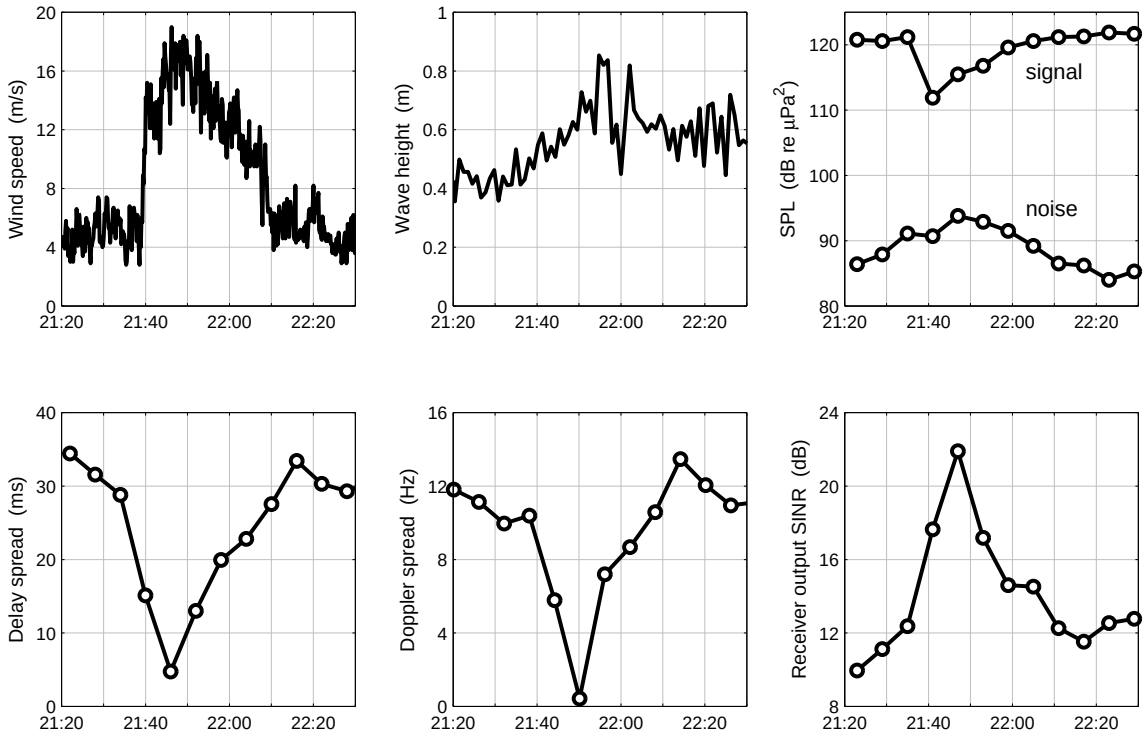

Figure 6.3 Effect of a wind burst on a communication channel

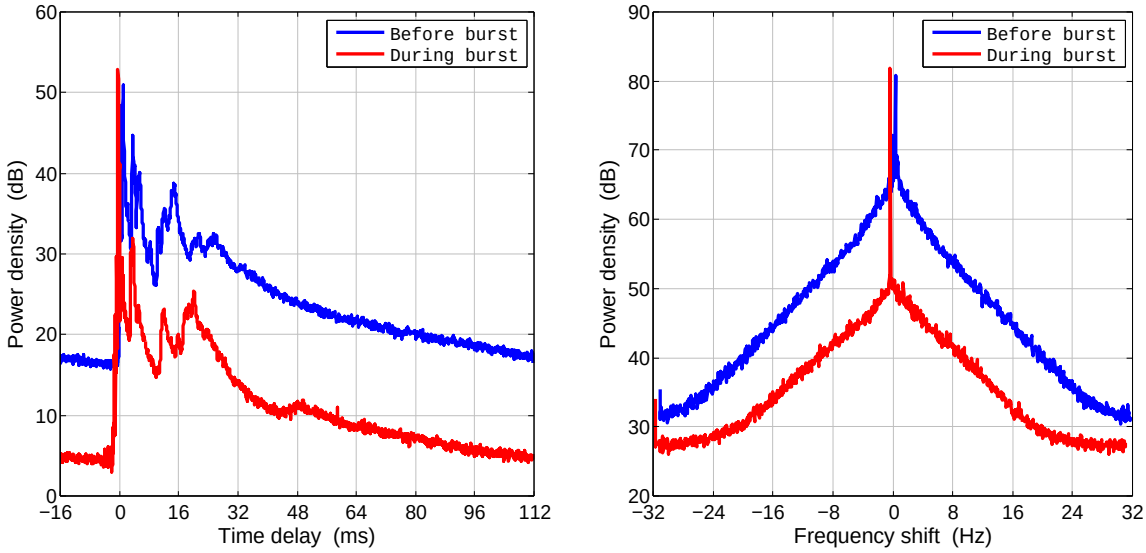

Figure 6.4 Power delay profile and Doppler spectrum measured before and during the wind burst. For clarity, a small offset is applied to separate the peaks at $\tau = 0$ and $\upsilon = 0$.

From Fig. 6.4 it is clear that $T = 32$ ms, used for Fig. 5.5, does not cover the reverberation tail. Worse, even $T = 128$ ms is too short. The blue profile is at least 12 dB above the noise floor, which can be seen from the part before $\tau = 0$, which is the cyclic continuation of the tail ending at $\tau = 112$ ms. Aliasing is unavoidable in Fig. 5.5, and also in Fig. 5.6 for that matter, whose true

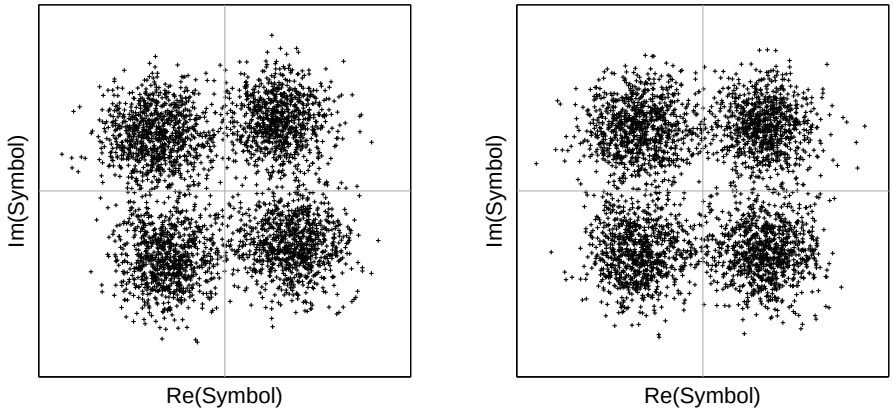

Figure 6.5 Channel G: constellations for an equalizer without (left) and with (right) PLL.

channel has a similar reverberation tail. However, this does not affect the points being made about these channels. The 32-ms soundings yield valid studies of the main arrivals, but note that the RMS and 90%-energy delay spreads in Table 5.2 are underestimates. The 32-ms probe has about 10% of its power aliased in delay, the 128-ms profile a much smaller fraction.

6.4 Phase drift in a stationary channel

The residual phase observed in Fig. 5.7 also has consequences for the communications receiver. Despite the static geometry, stationary environment, and accurate resampling to undo clock frequency offsets, the receiver faces a continuous phase drift because it tries to cling onto the bulk of the signal power. Without integrated phase-locked loop (PLL) [32] the equalizer cannot fully compensate for the phase drift, resulting in a rotation of the constellation: Fig. 6.5. To be sure, a PLL is useful when there are common phase drifts among multipaths. Channel G represents an atypically strong case. More often than not a PLL can be omitted in a static set-up.

7 Parameterization of Doppler spectra

There exists a big diversity of shapes of the shallow-water power delay profile, and in order to produce a realistic shape in simulations the simulator either needs to be of the replay type [4, 5], or an acoustic propagation model is required together with a comprehensive set of input parameters. The situation may be different for the Doppler spectrum.

7.1 Stretched and compressed exponentials

Five years of channel sounding in various areas and seasons have yielded Doppler power spectra, whose basic shape appears to be well described by [12]

$$P(v) \propto \mathrm{e}^{-\left(\frac{|v|}{\alpha}\right)^{\beta}}. \tag{7.1}$$

The stretching exponent β is a shape parameter that determines the peakedness of the spectrum and the heaviness of its tails. Eq. 7.1 is known as a stretched exponential when $\beta < 1$, a compressed exponential when $\beta > 1$, and conveniently includes the exponential ($\beta = 1$) and Gaussian ($\beta = 2$) power distributions. The stretched exponential is introduced as a basic shape, because power spectra additionally may have

- excess specular energy;
- spectral asymmetry;
- an offset;
- wave-spectrum sidelobes;
- distortion due to TX/RX motion.

It is of course also possible that spectra with a different basic shape exist, but so far Eq. 7.1 fits well to the majority of channels in FFI's archives. Upon fitting the stretched exponential to measured spectra, the offset can be taken into account. This leads to an equation with five fitting parameters

$$P(v) = A\mathrm{e}^{-\left(\frac{|v-v_0|}{\alpha}\right)^{\beta}} + n \,, \tag{7.2}$$

where A is just a scaling factor and n denotes the noise floor. At a given value of the shape parameter β, α is a measure of the Doppler spread. Fig. 7.1 shows four examples with various values of β. There are three stretched exponentials and one compressed exponential, which is the spectrum of channel D. A spectrum from the KAM08 experiment [31] is included ($\beta = 0.45$) to illustrate that the shape is not unique to Norwegian waters. The $\beta = 0.45$ and $\beta = 0.82$ spectra have excess power density at $v = 0$ due to specular paths. Since the curve fitting is performed in logarithmic space, this single outlier has little influence on the best-fit curve. However, such an outlier can represent a significant fraction of the total signal power and should not be ignored in simulations.

The spectral shifts that are sometimes encountered, even with bottom-mounted transceivers, have been measured previously [17], but typically for narrowband signals and a backscatter geometry. Scharf and Swarts [33] predict a frequency shift and a Gaussian spectrum for a rough sea. Exponents $\beta \approx 1.6$ are the closest to a Gaussian in FFI's sounding archives.

7.2 Narrowband spectra

A recent addition to FFI's channel sounding scheme is a sum-of-sines probe signal. These are simultaneously transmitted sine waves at a few discrete frequencies, permitting analysis of narrowband phenomena. They have the same frequency resolution as a PRBS or chirp train at the same total signal duration, a larger frequency-shift window, but very poor resolution in delay. A sine wave does not permit measurement of the time-varying impulse response, but can be used to extract narrowband signal fading statistics and Doppler spectra.

Figure 7.2 shows a wideband (10–18 kHz) Doppler spectrum measured with a PRBS, and narrowband spectra obtained for sine waves at five discrete frequencies evenly spread over the PRBS

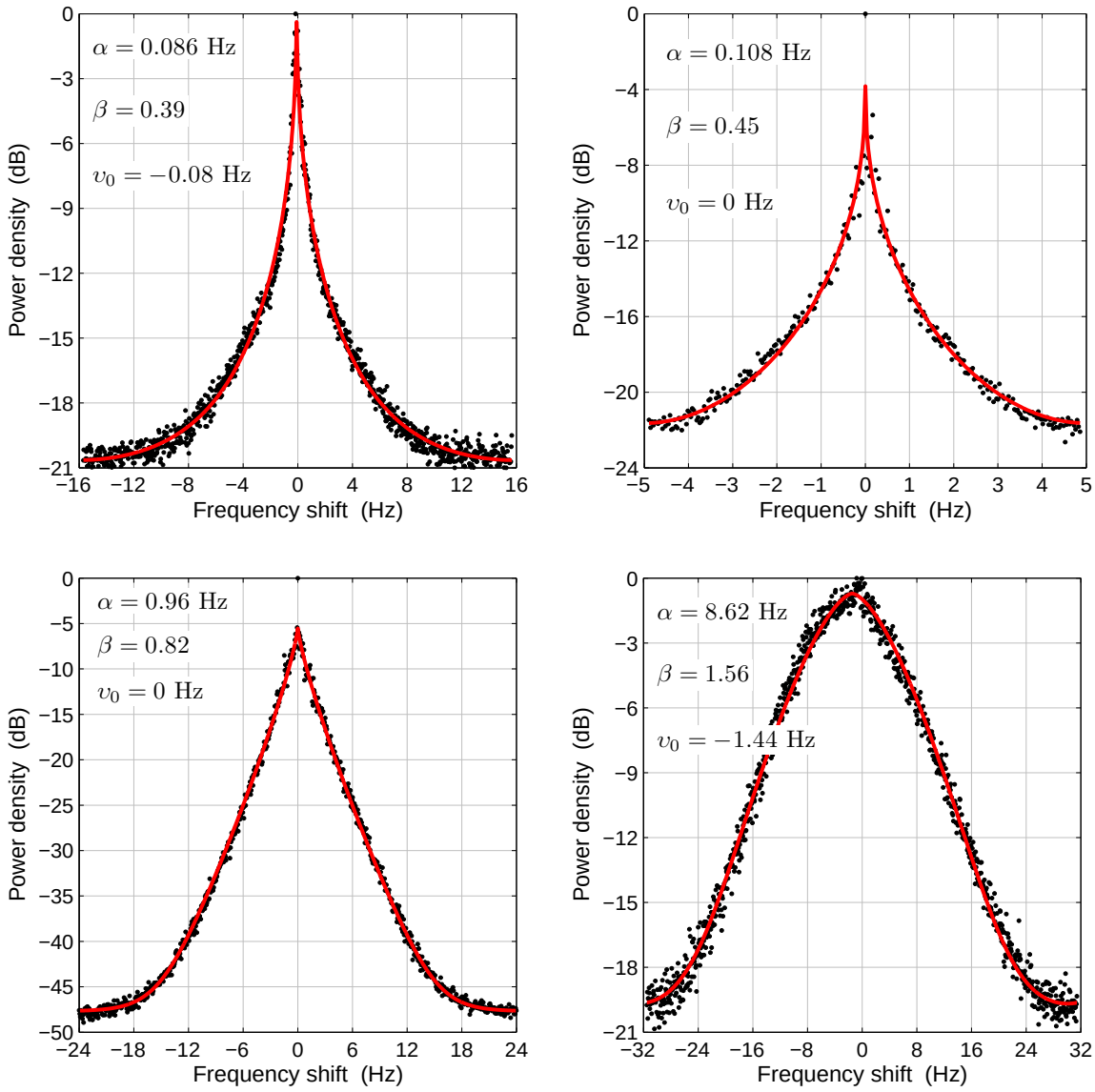

Figure 7.1 *Measured Doppler spectra and best-fit curves. The curve fitting takes into account spectral aliasing.*

band. Signaling is between bottom-mounted equipment and surface interactions are the predominant cause of Doppler spreading. The channel is considered stationary between transmission of the PRBS and the sum of sines, which are half a minute apart. Curve fitting yields a compressed exponential for all spectra with similar values of β. The next step is then to fix β at the wideband value of 1.31, repeat the curve fitting, and use α as a single measure of the Doppler spread. The noise floor differs between graphs, but the results clearly show that, within the uncertainty of channel stationarity and fitting accuracy: i) the Doppler spread increases linearly with the frequency; ii) the narrowband spectrum at the PRBS carrier frequency is characteristic of the wideband spectrum. The same conclusions were drawn for a stretched-exponential spectrum in [12].

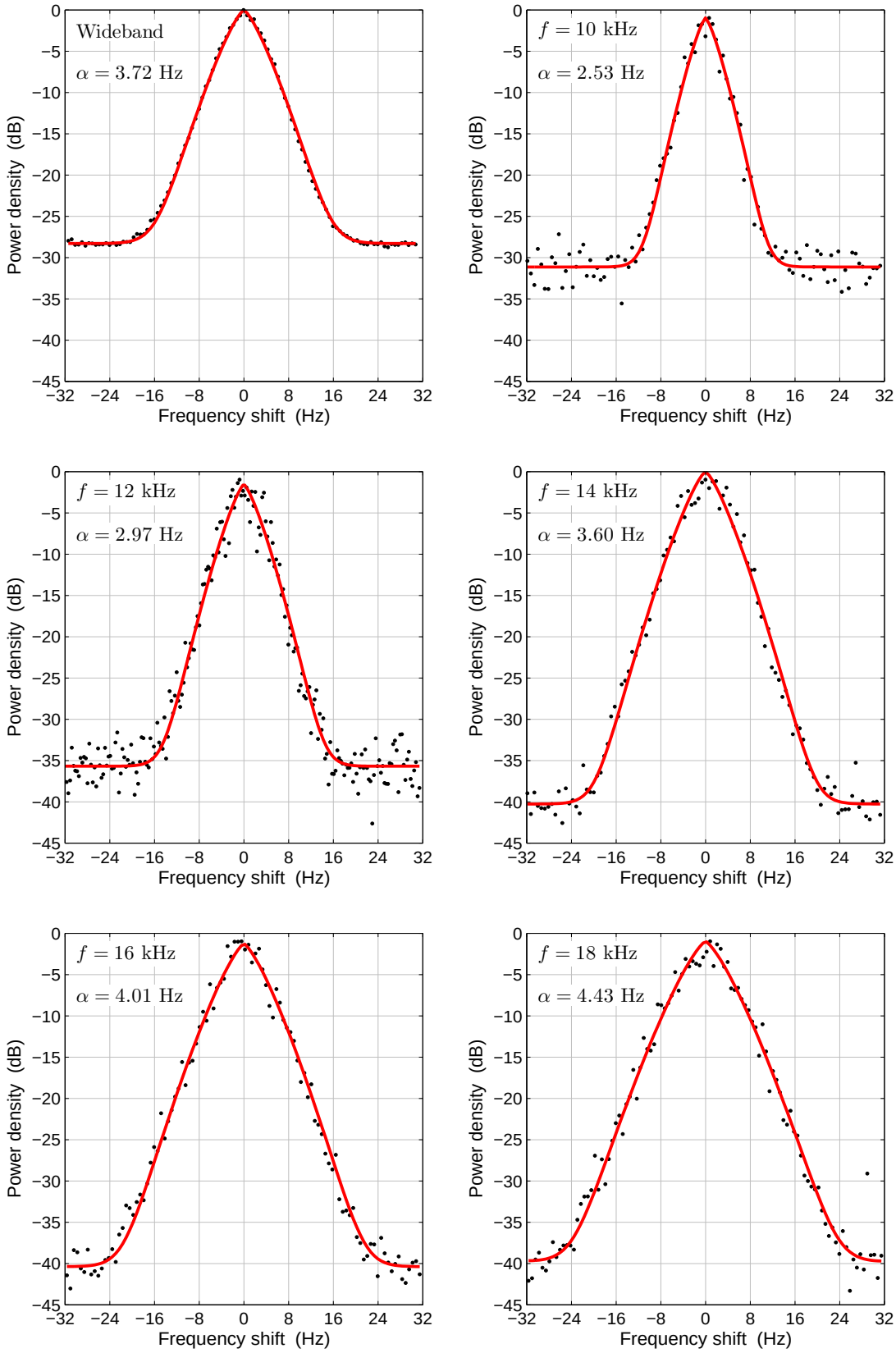

Figure 7.2 Wideband and narrowband spectra using β = 1.31 for all curves.

Similarly it can be shown that spectral shifts such as observed in channels D, F, and G are a function of the frequency. The fact that frequency spreads and shifts depend on the acoustic frequency is hardly surprising. However, one tends to forget this when working with wideband waveforms. Inspection of narrowband spectra creates awareness of the possible limitations of narrowband tools and models to characterize wideband systems. Different subbands of a wideband waveform may have different coherence times and fading rates. In the channel of Fig. 7.2 the coherence time is inversely proportional to the acoustic frequency. In retrospect, this casts doubt on many things presented in this report. All examined properties of the example channels may depend on the frequency, and the shown sounding results are averages over the frequency band of the probe signal. These results may be faithful averages that lead to valid conclusions, but awareness is required and channel models may need wideband ingredients, depending on the desired degree of completeness.

Note that frequency shifts due to TX/RX motion are (also) proportional to the acoustic frequency, but when all paths experience the same range rate the effects of motion can be mimicked or removed by resampling. Resampling is no instrument for Doppler spreading due to fading processes.

7.3 Relation between shape and width

Parameterization of Doppler spectra is a useful ingredient for stochastic channel simulation. Analysis of multiple spectra indicates that α and β (defined in Sec. 7.1) are not independent. Figure 7.3 plots α versus β for a collection of spectra obtained from channel soundings in Norwegian waters, combining data from three sites and two seasons. All these spectra are wideband (10–18 kHz) PRBS spectra which are well described by Eq. 7.2. The red line in the figure is a

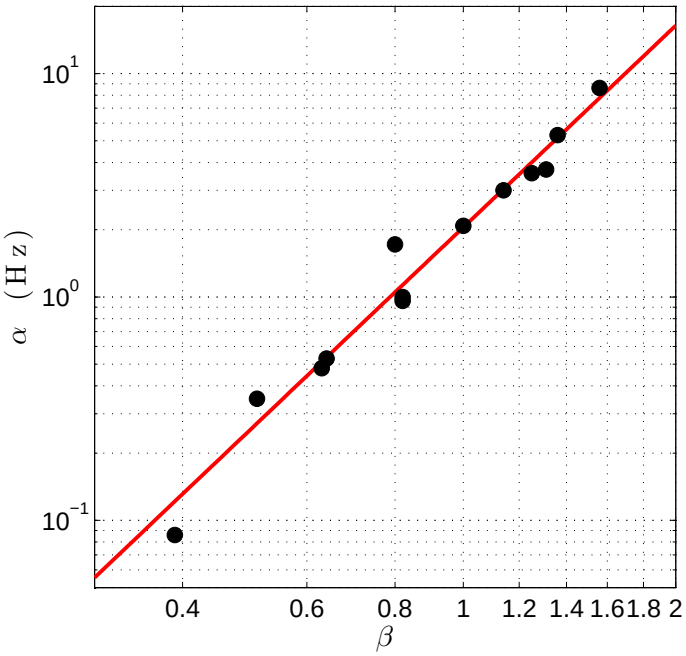

Figure 7.3 Apparent relationship between α and β at f_c = 14 kHz.

least-squares fit using $\alpha \propto \beta^3$. Since α was shown to be proportional to the frequency, this figure establishes an empirical relationship

$$\alpha \approx 1.5 \times 10^{-4} \beta^3 f \tag{7.3}$$

that seems to hold in Norwegian waters for 10 kHz $< f <$ 20 kHz. If such a relationship can be confirmed for soundings from more environments and frequency regimes, it reduces the stretched-exponential Doppler spectrum to a single parameter that is governed (at least for the data under consideration in the present report) by surface interactions.

Eq. 7.1 is phenomenological and physical explanations are not yet known. The wideband Doppler spectrum is generally an average over frequencies and over paths with different fading statistics. Summation of a distribution of broad and narrow spectra is perhaps expected to yield a sum with a sharp peak and heavy tails. Channel L illustrates this well. On the other hand, [12] shows that the stretched exponential also fits well to the spectrum of a single fading arrival. The shape of the spectrum in Fig. A.1 makes one wonder to what extent range-rate fluctuations contribute to measured spectra. With reflection and scattering of sound by waves, it is difficult to separate the contributions of multipath fading and small excursions in delay to the total Doppler spread.

8 Summary and conclusions

The technique of channel sounding and computation of channel parameters is described. Example channel measurements are shown for probe signals with a well-behaved cyclic autocorrelation function. This estimation method is simple, but sensitive to aliasing in two dimensions. When the characteristic time scale of channel fluctuations becomes of the order of the tracking period T or shorter, the choice of probe signal becomes important.

A diverse collection of example soundings highlights the diversity of acoustic propagation channels, illustrating the challenge to devise communication systems that are robust to the environment. It is also clear that channel simulation and modeling faces major hurdles and that assumptions, approximations, and simplifications limit the usefulness of a model to a subset of channels in existence. Regarding shallow-water communication channels, it can be said that

- Channels range from virtually ideal to overspread.
- Scattering can be correlated or uncorrelated.
- Scattering can be stationary, cyclostationary, or non-stationary.
- The scattering function can be separable or non-separable.
- Impulse responses can be sparse or densely populated.
- The most energetic arrival may be at the start of the impulse response, at the end, or somewhere in between.
- The power delay profile may have a seemingly endless reverberation tail with a non-negligible integral value.

- Arrivals can stay fixed on their tap, within the observable resolution B^{-1}, be subject to a time-varying time delay, or be scattered around some nominal value.
- Channel parameters such as delay spread, Doppler spread, and coherence time should be defined upon use. Much information is lost by reducing a time-varying impulse response to a few numbers.
- The question "What is the coherence time of the channel?" cannot always be answered.
- The shape of a subset of Doppler spectra is well represented by stretched and compressed exponentials. Deviations of the stretched exponential occur in the form of excess specular energy, spectral asymmetry and offsets, wave-spectrum sidelobes, distortion due to TX/RX motion.
- Frequency shifts due to continuous phase drifts, and asymmetrical spectra may occur even between bottom-mounted transmitters and receivers.
- Doppler spreading and frequency shifts depend on the acoustic frequency.
- Precise resampling is mandatory to separate Doppler effects due to channel dynamics on the one hand, and transceiver motion and clock frequency offsets on the other hand.
- TX/RX motion contributes to the Doppler variance and may dwarf the Doppler spread due to the medium itself. The opposite can also occur.
- TX/RX motion introduces time-varying range rates which may or may not differ between paths.

Nothing can be taken for granted. Good or bad results obtained in a shallow-water communication channel do not imply good or bad receiver performance. Until standard test channels are established, channel assessment should be a standard ingredient of publications in the field.

References

[1] D. B. Kilfoyle and A. B. Baggeroer, "The state of the art in underwater acoustic telemetry," *IEEE J. Oceanic Eng.*, vol. 25, no. 1, pp. 4–27, January 2000.

[2] M. Chitre, S. Shahabudeen, and M. Stojanovic, "Underwater acoustic communications and networking: recent advances and future challenges," *Marine Technology Society Journal*, vol. 42, no. 1, pp. 103–116, 2008.

[3] F. Guerra, P. Casari, and M. Zorzi, "World ocean simulation system WOSS: a simulation tool for underwater networks with realistic propagation modeling," in *WUWNet'09*, Berkeley, California, USA, November 2009.

[4] P. A. van Walree, T. Jenserud, and M. Smedsrud, "A discrete-time channel simulator driven by measured scattering functions," *IEEE J. Sel. Areas Commun.*, vol. 26, no. 9, pp. 1628–1637, December 2008.

[5] F.-X. Socheleau, C. Laot, and J.-M. Passerieux, "Stochastic replay of non-WSSUS underwater acoustic communication channels recorded at sea (submitted)," *IEEE Trans. Sig. Proc.*, 2010.

[6] G. Loubet and G. Jourdain, “Characterization of the underwater medium as an acoustical horizontal transmission channel,” in *OCEANS 1993*, Minneapolis, MN, USA, April 1993, pp. I329–I332.

[7] G. Cook and A. Zaknich, “Chirp sounding the shallow water acoustic channel,” in *ICASSP 1998*, vol. 4, Seattle, Washington, USA, May 1998, pp. 2521–2524.

[8] M. Chitre, J. Potter, and S. H. Ong, “Underwater acoustic channel characterisation for medium-range shallow water communications,” in *OCEANS 2004*, Kobe, Japan, November 2004, pp. 40–45.

[9] T. C. Yang, “Measurements of temporal coherence of sound transmissions through shallow water,” *J. Acoust. Soc. Am.*, vol. 120, no. 5, pp. 2595–2614, November 2006.

[10] T. C. Yang and W.-B. Yang, “High-frequency channel characterization for M-ary frequency-shift-keying underwater acoustic communications,” *J. Acoust. Soc. Am.*, vol. 120, no. 5, pp. 2615–2626, November 2006.

[11] B. Borowski, “Characterization of a very shallow water acoustic communication channel,” in *OCEANS 2009*, Biloxi, MS, USA, October 2009.

[12] P. van Walree, T. Jenserud, and R. Otnes, “Stretched-exponential Doppler spectra in underwater acoustic communication channels,” *JASA Express Lett.*, vol. 128, pp. EL329–EL334, November 2010.

[13] B. Tomasi, J. Preisig, G. B. Deane, and M. Zorzi, “A study on the wide-sense stationarity of the underwater acoustic channel for non-coherent communication systems,” in *European Wireless 2011*, Vienna, Austria, April 2011.

[14] D. Brady and J. C. Preisig, *Wireless communications: a signal processing perspective*. Prentice-Hall, March 1998, ch. 8, p. 330.

[15] D. E. Weston, K. J. Stevens, and M. Pengelly, “Multiple frequency studies of sound transmission fluctuations in shallow water,” *J. Sound Vib.*, vol. 18, no. 4, pp. 487–497, 1971.

[16] D. E. Weston and P. A. Ching, “Wind effects in shallow-water acoustic transmission,” *J. Acoust. Soc. Am.*, vol. 86, no. 4, pp. 1530–1545, October 1989.

[17] W. I. Roderick and R. L. Deavenport, “Doppler characteristics of sea surface reflected and scattered acoustic signals induced by surface wave motion,” in *OCEANS 1993*, Victoria, BC, Canada, October 1993, pp. I287–I292.

[18] J. C. Preisig and G. B. Deane, “Surface wave focusing and acoustic communications in the surf zone,” *J. Acoust. Soc. Am.*, vol. 116, no. 4, pp. 2067–2080, October 2004.

[19] S. A. Thorpe, “On the clouds of bubbles formed by breaking wind-waves in deep water, and their role in air-sea gas transfer,” *Phil. Trans. R. Soc. Lond. A.*, vol. 304, pp. 155–210, February 1982.

[20] M. V. Hall, "A comprehensive model of wind-generated bubbles in the ocean and predictions of the effects on sound propagation at frequencies up to 40 kHz," *J. Acoust. Soc. Am.*, vol. 86, no. 3, pp. 1103–1117, September 1989.

[21] M. A. Ainslie, "Effect of wind-generated bubbles on fixed range acoustic attenuation in shallow water at 1–4 kHz," *J. Acoust. Soc. Am.*, vol. 118, no. 6, pp. 3513–3523, December 2005.

[22] M. Stojanovic and J. C. Preisig, "Underwater acoustic communication channels: propagation models and statistical characterization," *IEEE Commun. Mag.*, vol. 47, no. 1, pp. 84–89, January 2009.

[23] M. A. Ainslie, *Principles of sonar performance modeling*, 1st ed. Springer-Verlag, 2010, pp. 414–415.

[24] P. van Walree, T. Jenserud, and H. Song, "Characterization of overspread acoustic communication channels," in *ECUA 2010*, Istanbul, Turkey, July 2010.

[25] G. Jourdain and J. P. Henrioux, "Use of large bandwidth-duration binary phase shift keying signals in target delay Doppler measurements," *J. Acoust. Soc. Am.*, vol. 90, no. 1, pp. 299–309, July 1991.

[26] T. Collins and P. Atkins, "Doppler-sensitive active sonar pulse designs for reverberation processing," *IEE Proc.-Radar Sonar Navig.*, vol. 145, no. 6, pp. 347–353, December 1998.

[27] P. A. Bello, "Characterization of randomly time-variant linear channels," *IEEE Trans. Commun. Sys.*, vol. 11, no. 4, pp. 360–393, December 1963.

[28] B. Sklar, *Digital Communications*, 2nd ed. Prentice Hall, 2001.

[29] M. P. Fitton, A. R. Nix, and M. A. Beach, "A comparison of RMS delay spread and coherence bandwidth for characterization of wideband channels," in *IEE Colloq. Propagation Aspects of Future Mobile Systems*, Biloxi, MS, USA, October 1996, pp. 9/1–9/6.

[30] P. van Walree, R. Otnes, G. Zappa, and J. Potter, "Comparison between JANUS and DSSS in Norwegian waters," in *UAM 2011*, Kos, Greece, June 2011.

[31] A. Song, M. Badiey, H. C. Song, and W. S. Hodgkiss, "Impact of source depth on coherent underwater acoustic communications (L)," *J. Acoust. Soc. Am.*, vol. 128, no. 2, pp. 555–558, August 2010.

[32] M. Stojanovic, J. A. Catipovic, and J. G. Proakis, "Phase-coherent digital communications for underwater acoustic channels," *IEEE J. Oceanic Eng.*, vol. 19, no. 1, pp. 100–111, January 1994.

[33] L. L. Scharf and R. L. Swarts, "Acoustic scattering from a stochastic sea surface," *J. Acoust. Soc. Am.*, vol. 55, no. 2, pp. 247–253, February 1974.

Appendix A Additional figures

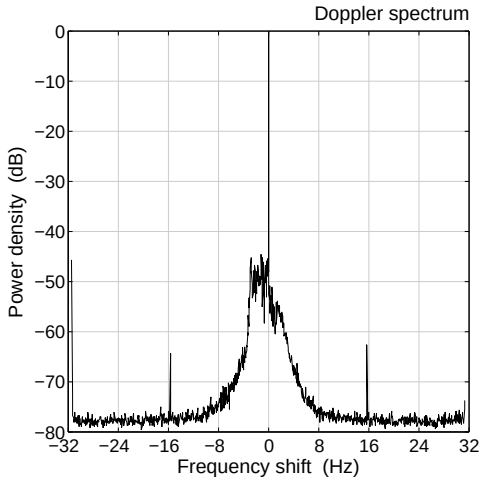

Figure A.1 *Spectrum of channel A, but obtained from a 16-ms PRBS. The extended observation window clearly shows the noise floor, as well as artifacts at* ± 16 *and* -32 *Hz.*

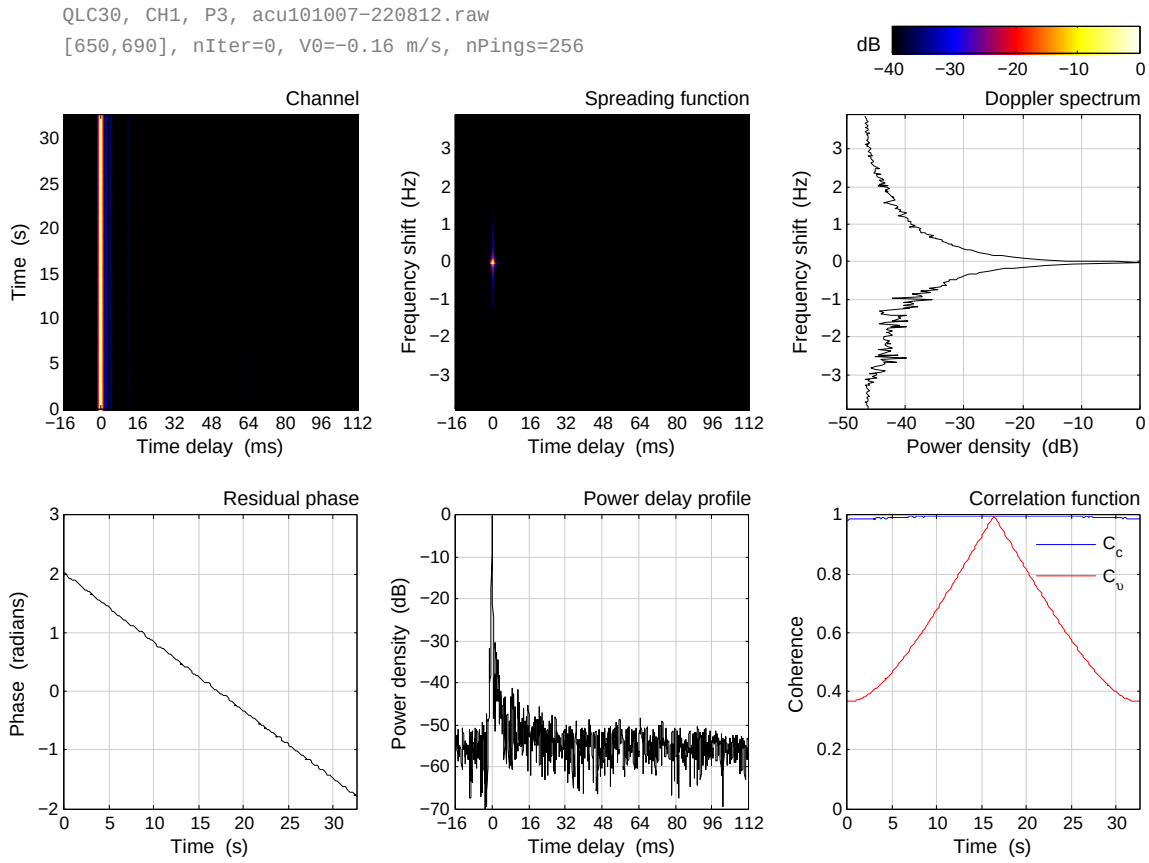

Figure A.2 *Channel A, but using* $V_0 = -0.16$ *m/s. The difference with Fig. 5.1 is a resampling factor of 1.0001067 instead of 1.0001054.*

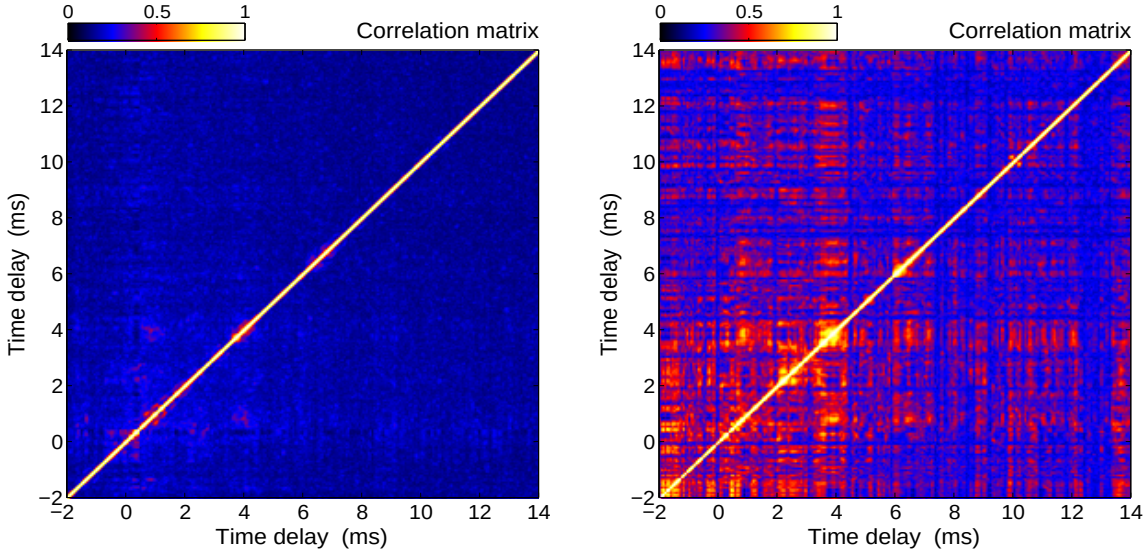

Figure A.3 Normalized correlation matrices for channels B (left) and C (right).

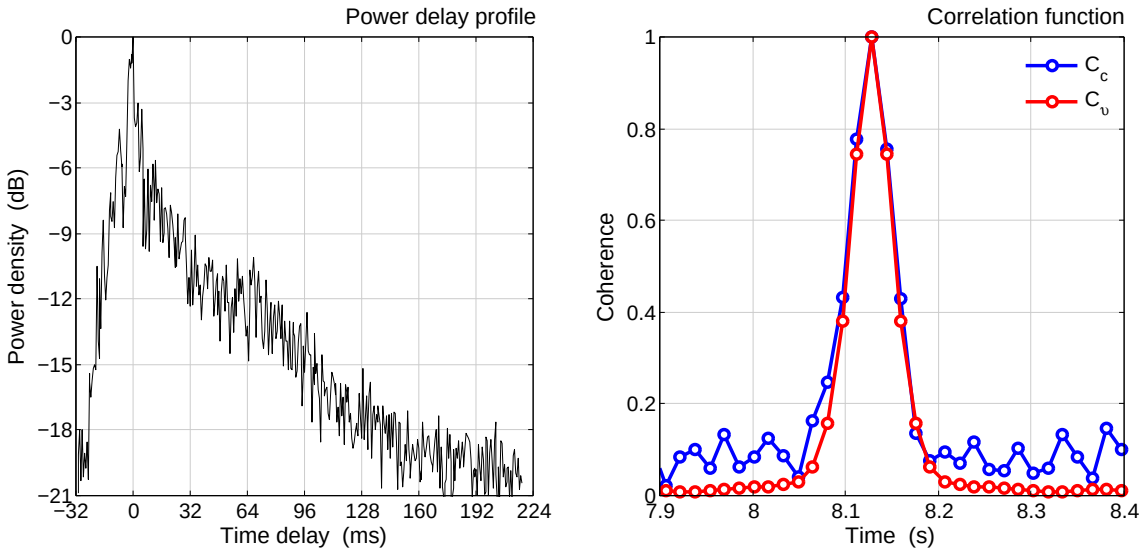

Figure A.4 Channel D functions are estimated with different probes. The figure zooms in on 16-ms PRBS correlation functions, whereas a 256-ms LFM probe is used for the delay profile. Table 5.2 combines the 16-ms Doppler spread and coherence time, and the 256-ms delay spread. Justification for this procedure is that these probes were transmitted within a two minutes of one another, whereas further measurements show that the channel is stationary over a longer period. Since the impulse response changes within a 256-ms LFM ping, the power delay profile suffers from the estimation errors illustrated by Fig. 4.2. This may affect the threshold delay spread, but should not have a noticeable effect on the RMS and 90%-energy values. The best strategy to measure the power delay profile in this channel would be sparse sampling: chirps with a duration $\leq$ 30 ms (the coherence time) and spaced by hundreds of milliseconds.

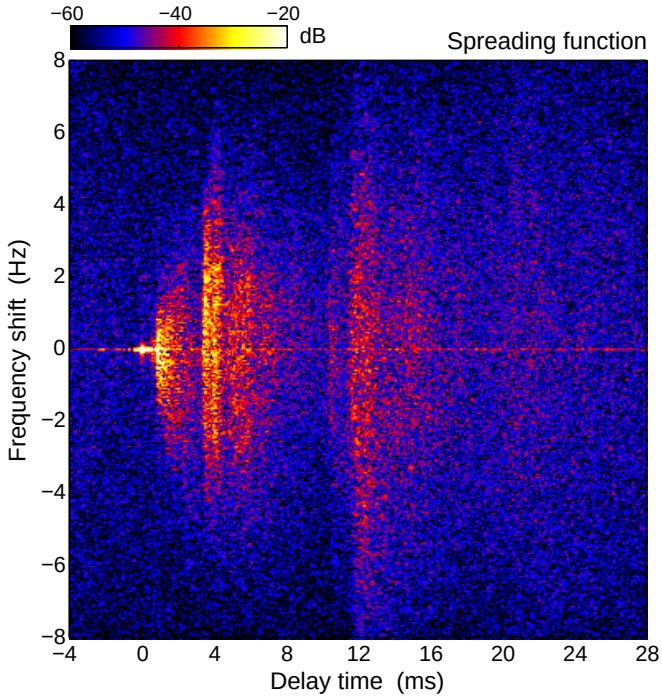

Figure A.5 *Spreading function of channel E. At this scale, the non-ideal PRBS autocorrelation function is evident from the sidelobes of the specular path.*

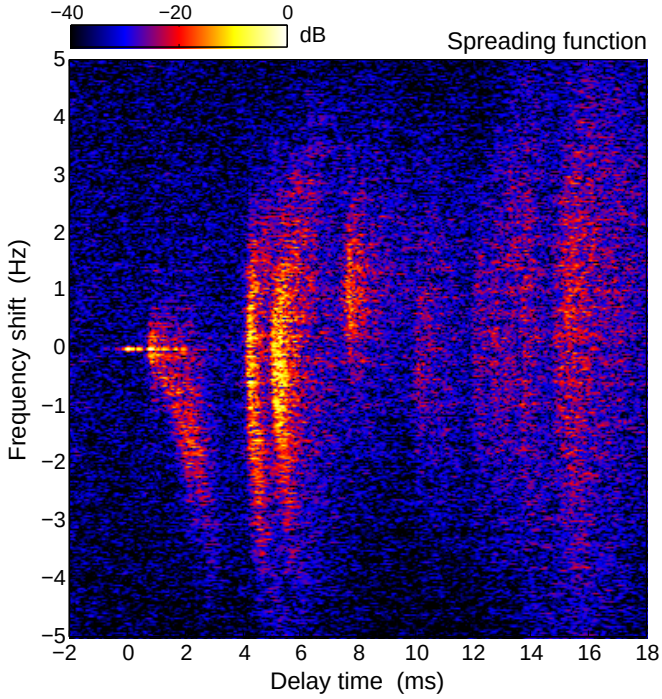

Figure A.6 *Spreading function of a channel featuring an arrival with a negative frequency shift, at $\tau = 2$ ms, and simultaneously an arrival with a positive shift, at $\tau = 8$ ms.*

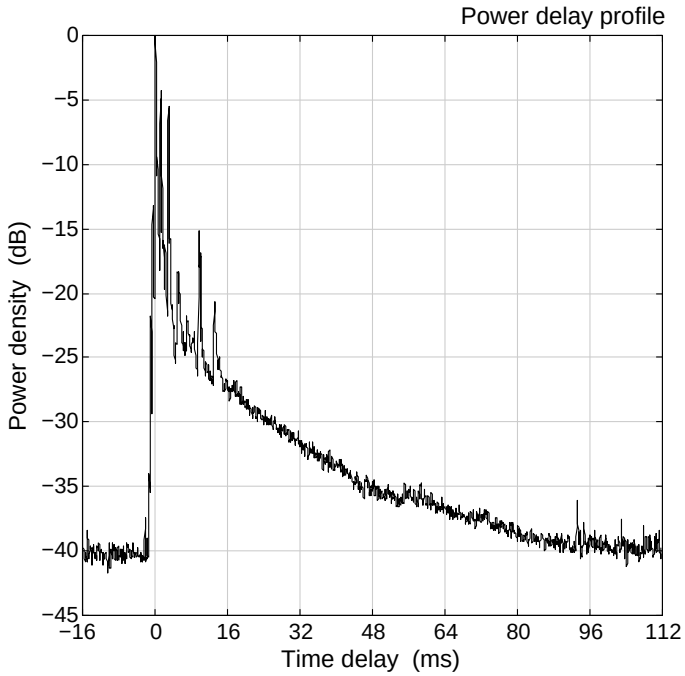

Figure A.7 Complete power delay profile for channel H.

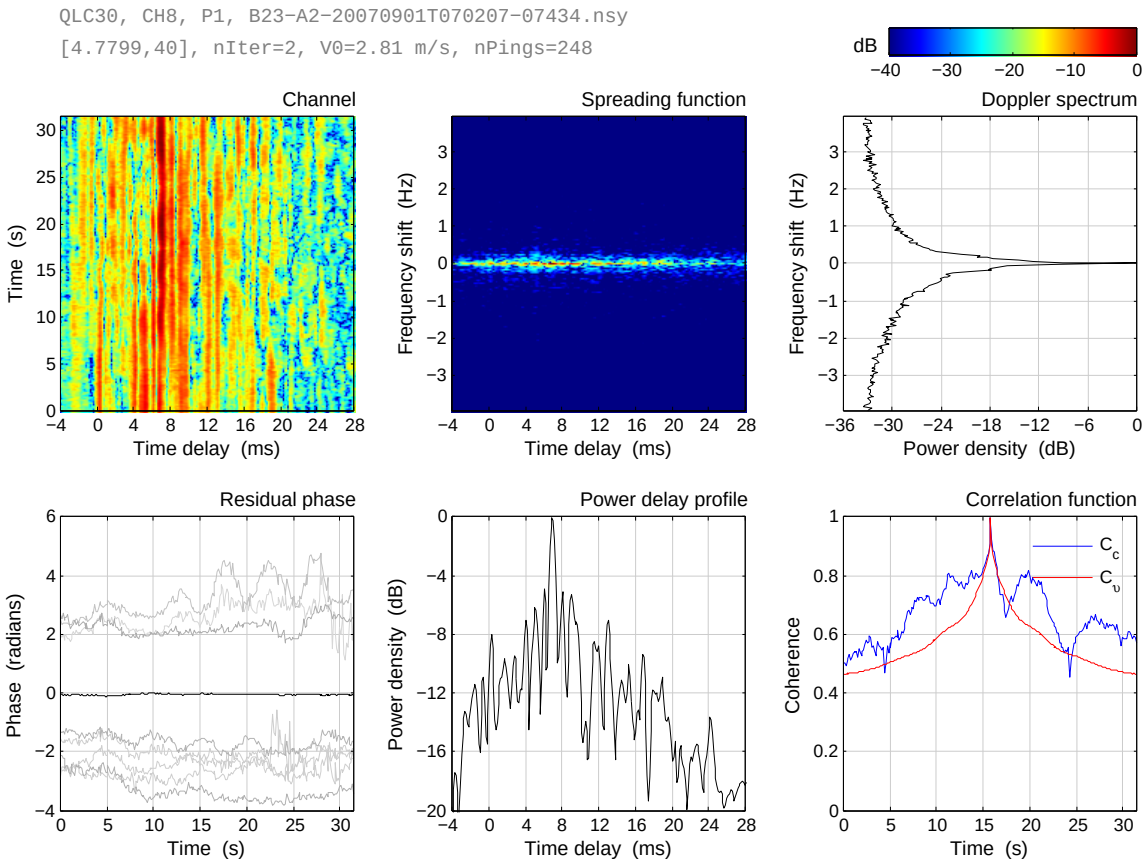

Figure A.8 Channel J.2, resulting from J by elimination of time-varying Doppler.

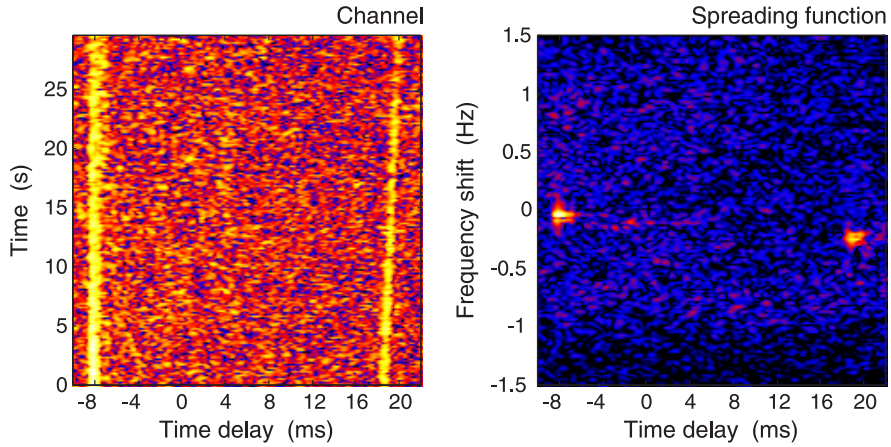

Figure A.9 *Channel K and its spreading function, but zoomed in on the first two arrivals. The first path is straight, the second one slanted.*

Abbreviations

BER	Bit Error Ratio
BPSK	Binary Phase-Shift Keying
DSSS	Direct Sequence Spread Spectrum
IFT	Inverse Fourier Transform
LFM	Linear Frequency Modulated
LMS	Least Mean Squares
PLL	Phase-Locked Loop
PRBS	PseudoRandom Binary Sequence
QPSK	Quadrature Phase-Shift Keying
RX	Receive
SINR	Signal-to-Interference-plus-Noise Ratio
SNR	Signal-to-Noise Ratio
SPL	Sound Pressure Level
TVD	Time-Varying Doppler
TX	Transmit

Acknowledgments

The author thanks the consortium and management group of the research project RTP 110.060 “UUV Covert Acoustic Communications”, and various colleagues at TNO, FFI and Kongsberg Maritime for enabling sea experiments and data acquisition. Hee-Chun Song is acknowledged for providing data snippets of the KAM08 experiment, Henry Dol for processing results from a recent Dutch/Norwegian sea trial, and Michael Ainslie for bringing attention of white horses and bubbles.